ORIGINAL RESEARCH

Nano-Ayurvedic Medicine Approaches Using *Ginkgo biloba*-Phytochemicals Functionalized Gold Nanoparticles Against Breast Cancer

Velaphi C Thipe [iD][1], Nya Hall[1], Amoolya Pandurangi[2], Samuel Ajayi [iD][3], Prosper Emeh[3], Iti Gauttam[3], Rania Ghamgui[3], Fatima Hameedat[3], Sihem Khelil[3], Nhu Ky Ly[3], Mahmoud Salim[3], Anum Shahid Waleed[3], Prajna Hegde[4], Vrushali Hegde[4], Deepa Prakash[4], Ilaadevi Hegde[4], Kavita Katti[1], Alice Raphael Karikachery[1], Emilie Roger [iD][3,5], Anne Landreau[3,6], Kattesh V Katti[1,7,8]

[1]Department of Radiology, University of Missouri, Columbia, MO, 65212, USA; [2]Department of Biology, Saint Louis University, St. Louis, MO, 63103, USA; [3]Pharmacy School, UNIV Angers, Angers, F-49000, France; [4]Kadamba Intrac Private Ltd, Bangalore, KA, 560011, India; [5]MINT, INSERM 1066, CNRS 6021, University of Angers, Angers, France; [6]Univ Angers, Univ Brest, IRF, SFR ICAT, Angers, F-49000 France; [7]Departments of Physics, Medical Pharmacology and Physiology, University of Missouri, Columbia, MO, 65211, USA; [8]Department of Biotechnology and Food Technology, University of Johannesburg, Doornfontein, 2028, South Africa

Correspondence: Kattesh V Katti, Department of RadiologyUniversity of Missouri-ColumbiaOne Hospital Drive, Columbia, Missouri, 65212, USA, Tel +1 573 882 5656, Fax +1 573 884 5679, Email KattiK@health.missouri.edu

Purpose: Breast cancer is a significant global health issue, contributing to 15% of cancer-related deaths. Our laboratory has pioneered a novel approach, combining Ayurvedic principles with green nanotechnology, to develop a scientifically rigorous medical modality referred to as Nano-Ayurvedic Medicine, recently approved by the US Patents and Trademarks Office. Here in we report a new Nano-Ayurvedic medicine agent derived from gold nanoparticles encapsulated with phytochemicals from *Ginkgo biloba* plant (GB-AuNPs).

Methods: We have developed biocompatible gold nanoparticles using electron-rich phytochemicals from *Ginkgo biloba* as reducing agent cocktail. *Ginkgo biloba* phytochemical-encapsulated gold nanoparticles (GB-AuNPs) were fully characterized, and their anticancer activity, including immunomodulatory profiles, were evaluated against breast (MDAMB-231) cancer cell lines.

Results: Characterization revealed spherical morphology for GB-AuNPs and possessed optimum in vitro stability through high zeta potential of -34 mV for optimum in vivo stability. The core size of GB-AuNPs of 19 nm allows for penetration into tumor cells through both EPR effects as well as through the receptor-mediated endocytosis. The Antitumor efficacy of this nano-ayurvedic medicine agent revealed strong antitumor effects of GB-AuNPs towards MDAMB-231. Our investigations reveal that GB-AuNPs enhance anti-tumor cytokines (IL-12, TNF-α, IFN-γ) and reduce pro-tumor cytokines (IL-10, IL-6), promoting the conversion of protumor M2 macrophages into M1-like macrophage antitumor phenotype. Cellular studies show that GB-AuNPs offer superior anti-tumor efficacy and a better safety profile against breast tumors compared to cisplatin.

Conclusion: Our investigations have demonstrated that the nano-ayurvedic medicine agent, GB-AuNPs, treats cancers through an immunomodulatory mechanism facilitated by elevated levels of anti-tumor cytokines (TNF-α, IFN-γ and IL-12) with concomitant downregulation of pro-tumor cytokines expression (IL-6 and IL-10). The green nanotechnology approach for the development of nano-ayurvedic medicine agent (GB-AuNPs), as described in this paper, presents new and attractive opportunities for treating human cancers and other debilitating diseases and disorders.

Keywords: *Ginkgo biloba*, gold nanoparticles, anticancer, Nano-Ayurvedic

Introduction

Ginkgo biloba L., also known as "Yin-xing" (Chinese), meaning "silver fruit", is a perennial plant belonging to the Ginkgoaceae family and it is one of the oldest living species on the planet. The ginkgo tree is a deciduous plant with green leaves that turn golden in autumn, and the seeds are contained in Ginkgo sarcotesta born on female trees.[1,2] This traditional Chinese herb is considered a living fossil as it has survived for over 250 million years without structural

modifications.[3,4] In the context of the sustainability and continuity of the plant kingdom, *Ginkgo biloba* epitomizes the most resilient plant species known to human civilization. Extracts from the leaves of Ginkgo have been used in ancient Indian Ayurvedic medicine and Chinese medicine for several thousand years to treat various diseases, including infectious lung diseases (eg, bronchitis) and cardiovascular diseases. Various studies have demonstrated the anticancer properties of edible plants (fruits, seeds, and leaves), which are attributed to the bioactive phytochemicals present in medicinal plants.[1] About 75% of the total fruit weight of edible plants, which are often discarded as waste, has been reported to exhibit significant anticancer activities.[1–7] *G. biloba* extracts have been reported to exhibit anticancer activity against a myriad of cancers.[5–8]

G. biloba is gaining greater attention and popularity in various regions of the world, and has become one of the most explored herbal medicinal products.[9–12] *Ginkgo biloba* is extensively cultivated worldwide, especially in Europe and the USA, owing to its recurrent beneficial antioxidant properties and highly promising pharmaceutical and medical applications.[13] Numerous studies have reported the beneficial properties of *G. biloba* leaf extract in improving blood circulation and reducing the risks of dementia and cognitive decline.[14,15] Modern phytochemical studies have demonstrated that leaf extracts contain hundreds of different bioactive compounds, including terpene lactones, flavonol glycosides, alkylphenols (ie, ginkgolic acids), flavonoids, fatty acids, proanthocyanidins, and polysaccharides.[5,16,17]

Several studies have investigated the standardized *G. biloba* leaf extract (EGb761, composed of 22–27% flavonoid glycosides, 2.8–3.4% terpene lactones (ginkgolides A, B, and C), and 2.6–3.2% bilobalide) as an effective anticancer drug (Figure 1).[12,18–23] These investigations have revealed that ginkgolic acids exhibit biological and pharmacological properties such as anti-inflammatory, antimicrobial, antiviral, and anticancer activities.[5,9,24]

Currently, there is growing interest in investigations focused on gaining insights on pharmacological mechanisms of phytochemicals derived from *G. biloba*.[25,26] Various commercial medicinal products are derived from *G. biloba*. However, variations in preclinical and clinical effectiveness have been demonstrated, in part due to differences in their composition, susceptibility to digestive enzymatic degradation, and poor bioavailability in vivo.[11,14,23,27,28] Recent pharmacological research has demonstrated that *G. biloba* possesses anticancer, antioxidant, anti-inflammatory, and immunomodulatory properties, thus demonstrating the importance of development new medically-valuable products for use in the treatment of various illnesses, with high specificity, safety, and efficiency.[23,26,29,30] The highly active surface area of gold nanoparticles allows embedding cocktail of bioactive phytochemicals on to the surface of AuNPs. Therefore,
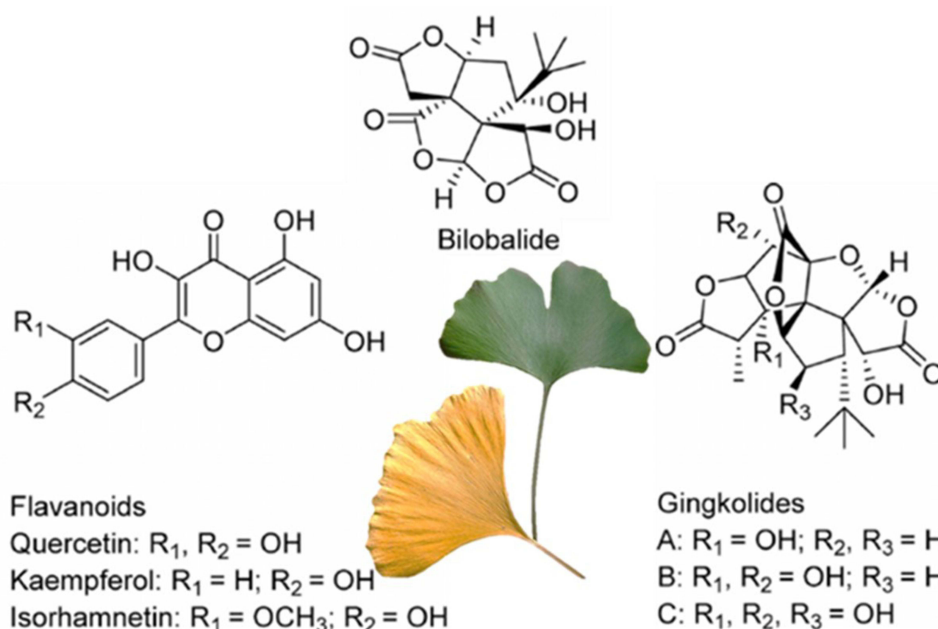

Figure 1 Key bioactive phytochemicals present in *G. biloba* leaf water-soluble extract. The major constituents include Bilobalide, Ginkgolides and Flavanoids, which contribute to the extract's therapeutic properties and potential biological activities.

this approach enables higher bioavailability of phytochemicals, from both targeting as well as therapeutic efficacy points of view, for use in cancer therapy.[31–35] As part of our ongoing efforts on the application of green nanotechnology towards the design and development of tumor-specific nanomedicine agents, Katti et al have pioneered the development of a myriad of phytochemical-functionalized gold nanoformulations with excellent preclinical and clinical efficacy.[36–61] In our pursuit of the application of green nanotechnology to ancient holistic Ayurveda medicine, Katti et al have recently discovered a new medical modality referred to as Nano-Ayurveda Medicine.[42–46,48,49,51,52,56,62] Herein, we report a green nano-ayurvedic approach for the synthesis *G. biloba* phytochemically-encapsulated gold nanoparticles (GB-AuNPs). We further report details of tumor specificity of GB-AuNPs against breast cancer (MDAMB-231 cancer cells). In addition, we have investigated whether GB-AuNPs exerted anti-inflammatory effects via inhibiting proinflammatory cytokines through the activation and promotion of anti-inflammatory cytokines by targeting macrophages using murine macrophage (RAW 264.7) cells within the tumor microenvironment. These studies provide evidence for the tremendous potential of GB-AuNPs as innovative immunomodulatory nano-ayurvedic agents for therapeutic interventions in treating cancers and various other inflammatory diseases.

Materials and Methods

All chemicals and reagents were purchased from Sigma-Aldrich Chemical Company (St Louis, MO, USA) and Thermo Fisher Scientific (Waltham, MA, USA) unless stated otherwise. 99% sodium tetrachloroaurate (III) dihydrate ($NaAuCl_4 \cdot 2H_2O$), in vitro stability biological media: phosphate-buffered saline (PBS), gum arabic (GA), DL-cysteine 97% (Cys), L-histidine 98% (His), sodium chloride (NaCl), Hanks' balanced salt solution (HBSS), bovine serum albumin (BSA), and lyophilized human serum albumin (HSA) powder were procured from Sigma-Aldrich (St Louis, MO, USA). Cellular stains 4',6-diamidino-2-phenylindole (DAPI), 3-(4,5-dimethylthiazol-2-yl)-2,5-diphenyltetrazolium bromide (MTT), wheat germ agglutinin (WGA), Oregon Green® 488 conjugate, and trypan blue were purchased from Sigma-Aldrich (St Louis, MO, USA). The positive control drug, cisplatin, was sourced from the US Pharmacopeia (Rockville, MD, USA). Cell culture: TrypLE Express was procured from Thermo Fisher Scientific (Waltham, MA, USA), while fetal bovine serum (FBS), gentamicin, Dulbecco's Modified Eagle Medium (DMEM), Roswell Park Memorial Institute (RPMI) 1640, vascular cell basal medium (VCBM), and endothelial cell growth kit-VEGF were obtained from Life Invitrogen (New York, NY, USA). Breast mammary gland adenocarcinoma (MDAMB-231), human aortic endothelial cells (HAEC), and murine macrophages (RAW 264.7) were obtained from the American Type Culture Collection (ATCC, Manassas, VA, USA).

Preparation of G. biloba Extract Solution

Leaves from female *G. biloba* tree were collected from a primitive tree at the Botanical Garden of the Department of Pharmacy, Faculty of Health, University of Angers, France. The plant was identified and authenticated by Anne Landreau, Professor of Botany. A voucher specimen (JBPA-108) with International Plant Exchange Network (IPEN) code XX-0-ANGMF-21 was deposited at the Herbarium of the Botanical Garden of the Department of Pharmacy, Faculty of Health, University of Angers, France. The *G. biloba* leaves were characterized and used for investigations at both the University of Angers, France and University of Missouri (Columbia, MO, USA). The leaves were thoroughly washed with water to eliminate potential contaminants. Subsequently, the clean leaves were air-dried and ground into fine powder using a mortar and pestle. Five grams of *G. biloba* powder was accurately weighed and added to a 100 mL flask containing 50 mL of deionized water. The mixture was heated at 80 °C for 15 min, the mixture was allowed to cool down to room temperature, centrifuged at 10,000 rpm for 15 min, and the supernatant was collected to obtain 100 mg/mL *G. biloba* water-soluble extract solutions containing water-soluble phytochemicals. The water-soluble extracts were used because our overarching goal of green nanotechnology has been to utilize aqueous media in the fabrication of *G. biloba* phytochemical encapsulated gold nanoparticles. Embedding *G. biloba* phytochemicals on gold nanoparticulate surface is expected to enhance the bioavailability of these therapeutic phytochemicals for further cancer therapeutic applications. Water insoluble parts were discarded.

Liquid Chromatography with Tandem Mass Spectrometry (LC-MS/MS) Liquid chromatography with tandem mass spectrometry (LC-MS/MS) analysis was performed on a Bruker maXis impact quadrupole-time-of-flight mass

spectrometer coupled to a Waters ACQUITY UPLC (ultrahigh performance liquid chromatography) system (UPLC-Q-TOF-MS/MS). Separation was achieved on a Waters C_{18} column (2 × 150 mm, BEH C_{18} column with 1.7 µm particles) using a linear gradient and mobile phases A (0.1% formic acid) and B (acetonitrile). The gradient conditions were as follows: B was increased from 5% to 70% over 30 min, then to 95% over 3 min, held at 95% for 3 min, and returned to 5% for equilibrium. The flow rate was 0.6 mL/minute, and the column temperature was 60 °C.

Mass spectrometry was performed in the positive electrospray ionization mode with the nebulization gas pressure at 44 psi, dry gas of 12 L/min, dry temperature of 250°C and a capillary voltage of 4000 V. Auto MS/MS Mass spectral data were collected using the following parameters: MS full scan: 100 to 1500 m/z; number of precursors for MS/MS: 3; threshold: 10 counts; active exclusion: 3 spectra, released after 0.2 min; collision energy: dependent on mass, 10 eV at 50 Da, 20 eV at 200 Da, 30 eV at 500 Da, 40 eV at 1000 Da, and 50 eV at 1500 Da. The MS and MS/MS data were auto-calibrated using sodium formate, which was introduced at the end of the gradient after the data acquisition.

G. biloba leaf extract was centrifuged at 13,000 × g for 15 min. After centrifugation, 2 µL of the supernatant was transferred to sample inserts and analyzed. Data were processed using the MetaboScape software (Bruker). Metabolites were putatively identified by matching their tandem spectral data against a custom tandem spectral library, 38 RIKEN spectral library, and NIST20 high-resolution accurate mass library. Multivariate analysis was performed using the Metabo Analyst software.

Green Synthesis of G. biloba Gold Nanoparticles (GB-AuNPs)

The synthesis of gold nanoparticles using aqueous extracts of *G. biloba* (GB-AuNPs) was optimized with repeated synthesis until we achieved 100% reproducibility (at least triplicates with various concentrations of leaf extracts). Briefly, to a scintillation vial, 12 mg of gum arabic was added and dissolved in 6 mL solutions containing different concentrations of the *G. biloba* extract solutions from the stock preparations (with *G. biloba* weights of: 100, 50, 25, 12.5, 6.25, 3.125, 1.56 mg/mL). The solutions were stirred at 700 rpm for 15 min at 90 °C, to this mixture, 100 µL of 0.1 M $NaAuCl_4.2H_2O$ was added. The reaction mixture turned ruby red, indicating transformation of gold precursor into the corresponding GB-AuNPs gold nanoparticles. The *G. biloba* gold nanoparticles (GB-AuNPs) were washed twice by centrifugation and resuspended in distilled water.

Optical Properties

The optical properties of GB-AuNPs were measured by diluting 200 µL of GB-AuNPs in 800 µL of distilled water in a disposable cuvette. Surface plasmon resonance spectra of GB-AuNPs were recorded using a Cary 60 UV–vis spectrophotometer (Agilent Technologies, Santa Clara, CA, USA).

Dynamic Light Scattering

The hydrodynamic size and zeta potential were measured using a Zetasizer Nano ZS (Malvern Panalytical Inc., Westborough, MA, USA). All measurements were recorded in triplicate.

Transmission Electron Microscopy (TEM)

TEM was used to investigate the core size, by placing 5 µL of GB-AuNPs onto a 200-mesh carbon support film (TEM grid) (Electron Microscopy Sciences, Hatfield, PA, USA) and allowed to air-dry. TEM grids were visualized using a JEOL 1400 TEM 120 kV (JEOL Ltd., Peabody, MA, USA). TEM images were subsequently processed using Image J. JS software to determine the particle size distribution.

Fourier-Transform Infrared Spectroscopy (FTIR)

Phytochemical conjugation and the identity of phytochemical encapsulated AuNPs were assessed using Fourier-transform infrared spectroscopy (FTIR). Approximately 40 mL of gum arabic-stabilized *G. biloba* phytochemical-encapsulated gold nanoparticles (GB-AuNPs) was poured into a standard borosilicate petri dish (100 mm × 15 mm) and then kept in an oven overnight at 100 °C for drying. The dark black dried nanoparticle residue was scraped

using a spatula, and ~60 mg was collected into a vial. This dry gold nanoparticle residue was milled with anhydrous KBr to prepare homogenous transparent pellets for FTIR analysis, following a conventional high-pressure approach using a hand-operated mini-press. A Thermo Scientific Nicolet Summit PRO FTIR Spectrometer, along with an iD1 transmission accessory for sampling, was used to collect the FTIR measurements. The spectra represent an average of 16 scans in the 4000–400 cm^{-1} spectral region and were collected at a resolution of 4 cm^{-1}. Background correction was performed with an accessory in place using a neat KBr pellet.

Powder X-Ray Diffraction (PXRD)

The crystalline characteristics of GB-AuNPs were assessed by powder X-ray diffraction (PXRD). GB AuNPs (40 mL GB AuNPs were poured into a standard borosilicate Petri dish (100 × 15 mm) and then kept in an oven overnight at 100 °C for drying. The dark black dried nanoparticle residue was scraped using a spatula, and ~60 mg was collected into a vial. Dry nanoparticle residue was used in the analysis. PXRD of the solid samples was performed using a Rigaku Miniflex diffractometer (Rigaku Americas Corporation, The Woodlands, TX, USA) equipped with a D-tex Ultra one-dimensional position-sensitive detector using Ni-filtered Cu Kα radiation (λ = 1.54060 Å, beam power = 45 kV, 20 mA). Depending on sample volume, samples were loaded into either a proprietary zero-background crystalline silicon background holder, with a 0.2 mm x 1.5 mm cylindrical well, or on top of a glass substrate in a larger aluminum sample holder. Diffraction data were measured in continuous 2-theta scanning mode at a rate of 2.00°/min and step size of 0.02° with beta rotation at a rate of 80 RPM. The background signal from the glass substrate was subtracted using a polynomial fit calculated using Rigaku SmartLab Studio II (*SmartLab Studio II*, version 4.6.671.0, Rigaku Corporation, Tokyo, Japan, 2014).

In vitro Stability Analysis of GB-AuNPs

In vitro stability of GB-AuNPs was investigated by monitoring the surface plasmon resonance (SPR) peak over time in various biological media. Briefly, a 1:2 volume ratio of GB-AuNPs was incubated in various biological media, including PBS, buffered solutions at pH 4, 7, and 10, 0.5% BSA, 0.5% HSA, 0.5% Cys, 0.2% His, and nutrient media (RPMI and DMEM) solutions. GB-AuNPs were incubated in various solutions as described above for a month and subsequently SPR peak was monitored using UV–vis spectrophotometry. Additionally, in separate experiments, GB-AuNPs was incubated in various biological media mentioned above, for a week. The stability of GB-AuNPs was investigated by measuring the size differences using the Zetasizer Nano and electron microscopy (TEM).

Cellular Investigation of GB-AuNPs on Cells

Breast mammary gland adenocarcinoma cells (MDAMB-231), human aortic endothelial cells (HAEC), and murine macrophages (RAW 264.7) were obtained from the American Type Culture Collection (ATCC, Manassas, VA, USA). Cells were all cultivated following standard aseptic work procedures in the laminar flow and cultured in an incubator at 37 °C in 95% air and 5% CO_2. MDAMB-231 and RAW 264.7, cells were cultured in Dulbecco's modified Eagle's medium (DMEM) supplemented with 10% fetal bovine serum and 1% penicillin-streptomycin. Vascular cell basal medium (VCBM) supplemented with the endothelial cell growth kit-VEGF was used to culture HAEC.

Cell Viability MTT Assay

The cellular viability of GB-AuNPs was investigated using the MTT Formazan cell proliferation assay (Sigma-Aldrich, St Louis, MO, USA) to determine their anticancer activity against the breast cancer cell line (MDAMB-231) and their activity against normal cells (HAEC). Briefly, 100 μL of 5×10^4 cells/mL of each cell line was seeded in 96-well cell culture plates and incubated in a 5% CO_2 incubator at 37 °C overnight. After incubation, the media were aseptically removed and replaced with culture media containing GB-AuNPs (200, 100, 50, 25, 12.5, and 6.25 μg/mL); negative control: untreated cell media only and positive control: cisplatin (200, 100, 50, 25, 12.5, and 6.25 μg/mL). The plates were then incubated for 24, 48, and 72 h. Thereafter, 10 μL of MTT reagent (5 mg/mL in PBS) to each well was added and the plates were incubated for 3–4 hr at 37 °C to allow the formation of formazan crystals, the MTT solution was removed, and formazan crystals were

dissolved in 100 μL of DMSO. The absorbance of the purple formazan crystals was measured using a SpectraMax M2 microplate reader (Molecular Devices LLC, San Diego, CA, USA) operating with the plate gently shaken for 15s, prior to recording at a wavelength of 570 nm.

The percentage of viable cells was determined using the following equation (Equation 1):

$$\% \text{Cell Viability} = \frac{(T_{Ab} - B_{Ab})}{(C_{Ab} - B_{Ab})} \times 100$$

where T_{Ab} is the absorbance of the treatment, B_{Ab} is the absorbance of the blank (medium) and C_{Ab} the absorbance of the control (untreated cells). The half-maximal inhibitory concentration (IC_{50}) was calculated using GraphPad Prism Version 10.0.2.

Cellular Internalization of GB-AuNPs

Initially, ultraclean and sterile coverslips were placed in six-well plates. Subsequently, 8×10^5 cells per well were seeded in appropriate media (DMEM for MDAMB-231 and RAW 264.7, and VCBM for HAEC cells) and cultivated for 24 h at 37 °C in a 5% CO_2 incubator. After this incubation period, the culture medium was removed and replaced with media containing 50 μg/mL of GB-AuNPs, followed by an additional 24 hr incubation at 37 °C.

Post-incubation, the cells underwent a series of procedures: they were rinsed three times with 1X HBSS, stained with 2 μg/mL of WGA to highlight the cytoplasm, and incubated for 10 min at room temperature in darkness. The cells were washed twice with 1X HBSS and permeabilized using 0.2% Triton X-100 at room temperature for 5 min. The cells were again washed twice with 1X HBSS and stained with 1 μg/mL DAPI to visualize nuclei. The slides were monitored using a Leica TCS SP8 STED confocal microscope (Leica, Wetzlar, Germany) at 40x magnification, and the Dage Imaging Software was used for image collection.

In parallel, Cells (at a density of 8×10^5 cells/mL) were cultured in six-well plates, washed with 1X PBS, and incubated for 24 h at 37 °C with media containing 50 μg/mL of GB-AuNPs. Following this incubation, the cells were washed with 1X PBS, dislodged using Tryple E for 3 min, and trypsinization was halted by adding media. The cells were subsequently collected into 1 mL Eppendorf tubes, centrifuged, and washed with 1X PBS at 1000 rpm for 5 min. The cell pellets were then treated with a mixture of 2% glutaraldehyde and 2% paraformaldehyde in 0.1 mm sodium cacodylate buffer. Subsequently, the cells were exposed to 1% osmium tetroxide in 2-mercaptoethanol, dehydrated using a series of acetone concentrations, and embedded in Epon-Spurr epoxy resin. Thin sections approximately 85 nm thick were sliced using a diamond blade (Diatome, Hatfield, PA, USA).

For organelle visualization, sections were stained with Sato's triple lead stain and 5% aqueous uranyl acetate. The prepared samples were analyzed using a JEOL 1400 TEM microscope (JEOL, Peabody, Massachusetts, USA) operating at 80 kV, at the electron microscopy core facility of the University of Missouri-Columbia.

Statistical Analysis

GraphPad Prism Version 10.0.2 software (GraphPad Software, San Diego, CA, USA) was used to conduct statistical analysis. Using the two-way ANOVA test, statistical evaluation was conducted to determine the efficacy of the treatment. To compare the average of the treatment group to the average of the control group, IC_{50} values was calculated. With $p < 0.05$ statistical tests were deemed significant. All results are shown as the mean standard error of the mean.

Results
Chemical Composition of G. biloba by LC-MS/MS

LC-MS/MS data revealed that the major phytochemical constituents were quinic acid, polyalcohols, xanthurenic acid, glycosides, and quercetin-based compounds (Figure 2). The polyalcohols included pinitol and opuntiol. The glycosides present were luteolin-7,3'-di-O-glucoside, luteolin-4'-O-glucoside, kaempferol-7-O-glucoside, kaempferol-3-O-rutinoside, and narcissin D-glucopyranoside derivatives and many others. Quercetin and related compounds such as isoquercitrin and quercetin 3-glucoside-7-rhamnoside were also observed. The LC-MS/MS phytochemical composition profile of *G. biloba* extract is shown in Figure 3.
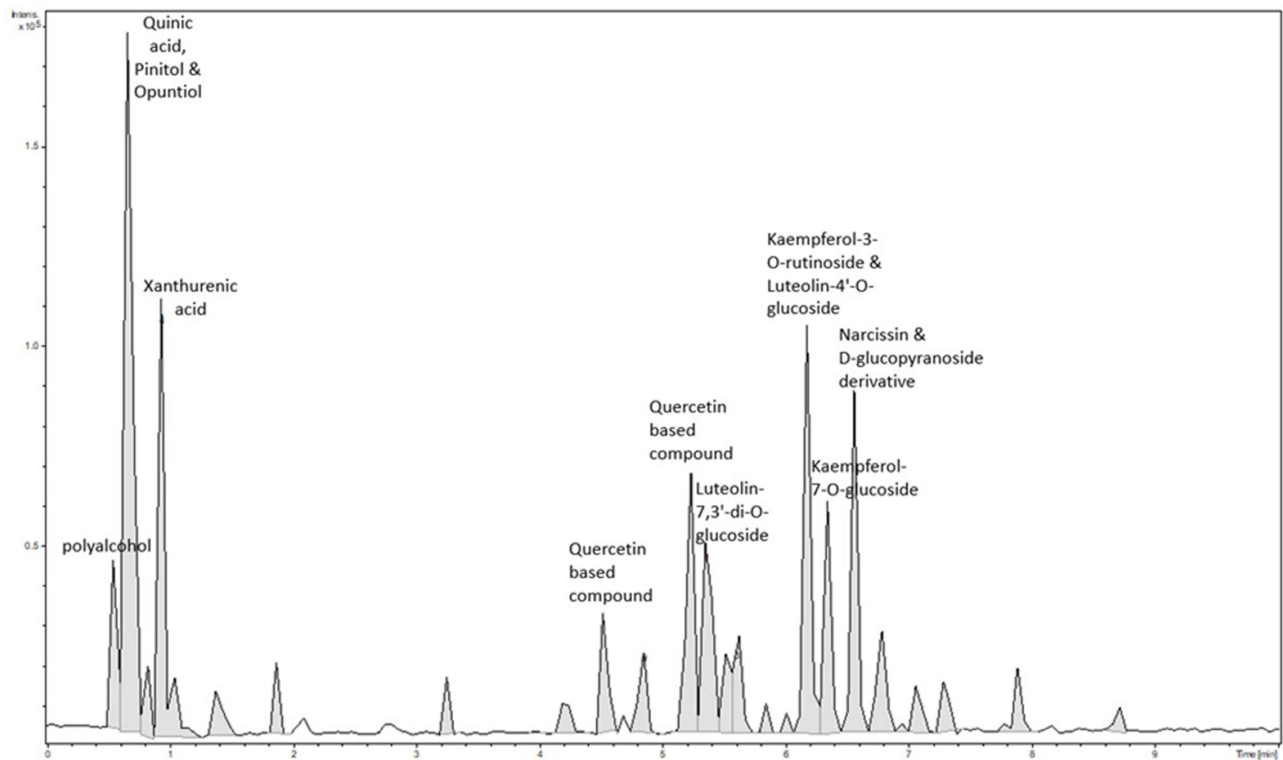
194

Nanotechnology, Science and Applications 2024:17

Figure 2 LC-MS/MS spectra of *G. biloba* aqueous extract, highlighting the detection of key phytochemical constituents. The primary compounds identified include quinic acid, polyalcohols, xanthurenic acid, glycosides, and quercetin-based compounds, each contributing to phytochemical-rich extract's bioactive profile.
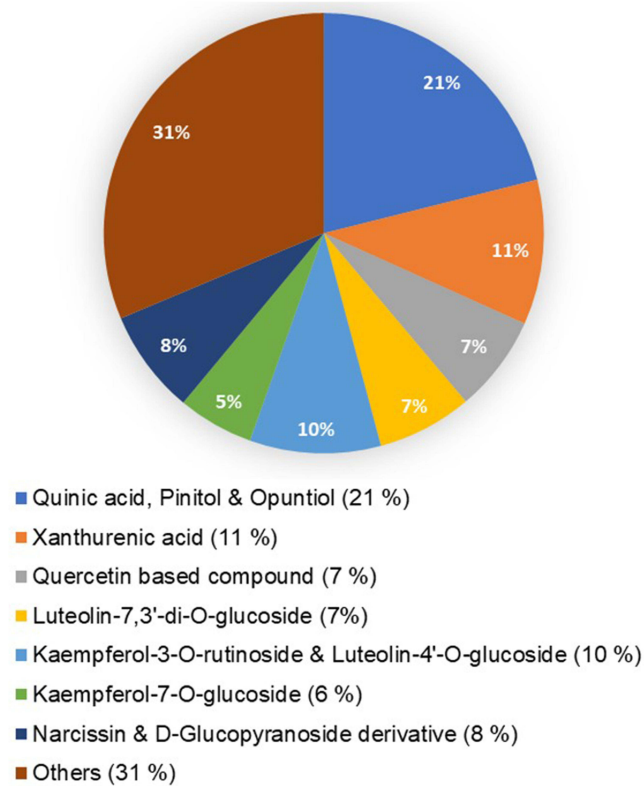

- ■ Quinic acid, Pinitol & Opuntiol (21 %)
- ■ Xanthurenic acid (11 %)
- ■ Quercetin based compound (7 %)
- ■ Luteolin-7,3'-di-O-glucoside (7%)
- ■ Kaempferol-3-O-rutinoside & Luteolin-4'-O-glucoside (10 %)
- ■ Kaempferol-7-O-glucoside (6 %)
- ■ Narcissin & D-Glucopyranoside derivative (8 %)
- ■ Others (31 %)

Figure 3 Pie chart depicting phytochemical composition of *G. biloba* aqueous extract as determined by LC-MS/MS analysis, illustrating relative abundance of key bioactive compounds.

UV-Vis Spectroscopy and Physicochemical Properties of GB-AuNPs

The successful synthesis of GB-AuNPs was evident from the transformation of yellow gold precursor solutions into vibrant ruby-red color upon addition of aqueous extracts from Ginkgo biloba phytochemicals cocktails to reaction mixtures. The characteristic surface plasmon resonance (SPR) peaks between 535–555 nm (Figure 4b) further confirmed the presence of GB-AuNPs. We have evaluated the SPR peaks, hydrodynamic size, polydispersity index (PDI), and zeta potential of GB-AuNPs at various concentrations (with *G. biloba* weights: 100, 50, 25, 12.5, 6.25, 3.125, and 1.56 mg/mL) as shown in Figure 4a–d. Detailed analysis of physiochemical data indicated that 6.25 mg/mL concentration of *G. biloba* was optimal for the production of excellent quality gold nanoparticles— exhibiting a zeta potential of −34 mV and a PDI of 0.3. These data were reproduced numerous times and signify superior stability and monodispersed compositions of GB-AuNPs as compared to data obtained when various other concentrations of *G. biloba* were used. Therefore, we selected the 6.25 mg/mL as the most optimum concentration of *G. biloba* for the production of GB-AuNPs for further investigations and henceforth we have referred these particles as GB-AuNPs. The cocktail of antioxidant phytochemicals present in *G. biloba*, particularly polyphenolics, exhibit reducing capabilities that enable them to act as primary reducing and polar agents. As shown in Scheme 1, quercetin, a major antioxidant, played a crucial role in the reduction of GB-AuNPs. However, it is important to note that other phytochemicals also contribute to this process. The reduction of Au ions to GB-AuNPs occurs through oxidation of the hydroxyl (–OH) group of phytochemicals. Additionally, other phytochemicals, such as kaempferol, isorhamnetin, bilobalide, and ginkgolides form a thin layer on the particle surface, thereby aiding reduction while stabilizing the nanoparticles. In order to assess the in vitro stability of GB-AuNPs, nanoparticles were subjected to various biological media, including 0.5% BSA, HSA, and Cys, 0.2 M His, 1% NaCl, RPMI and DMEM media, PBS
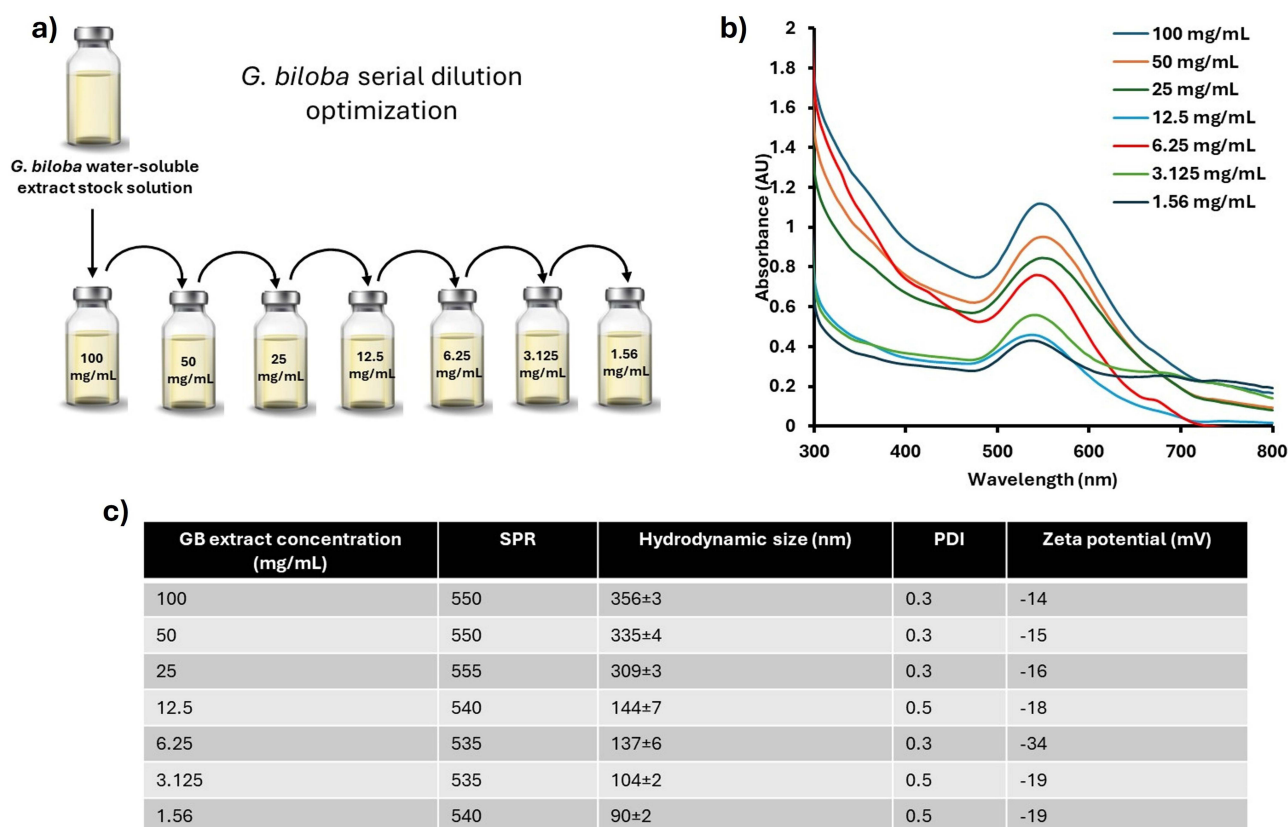

GB extract concentration (mg/mL)	SPR	Hydrodynamic size (nm)	PDI	Zeta potential (mV)
100	550	356±3	0.3	-14
50	550	335±4	0.3	-15
25	555	309±3	0.3	-16
12.5	540	144±7	0.5	-18
6.25	535	137±6	0.3	-34
3.125	535	104±2	0.5	-19
1.56	540	90±2	0.5	-19

Figure 4 Synthetic parameters of GB-AuNPs: (**a**) Serial dilution of *G. biloba* stock solution to achieve varying concentrations, (**b**) Ultraviolet-visible spectra of GB-AuNPs synthesized from different concentrations of *G. biloba* extract, demonstrating the influence of extract concentration on nanoparticle formation, and (**c**) Physicochemical properties of GB-AuNPs at different extract concentrations, highlighting variations in size, polydispersity index (PDI), and surface charge.

196

Nanotechnology, Science and Applications 2024:17
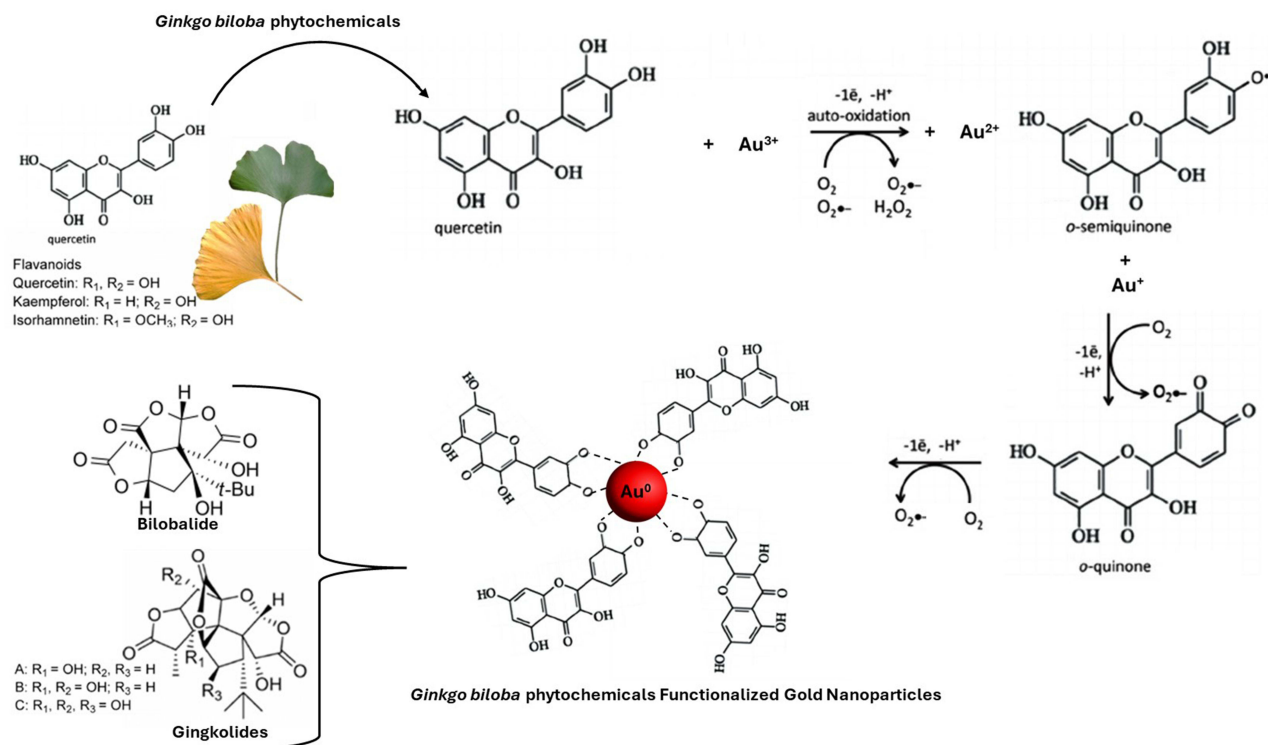
Scheme 1 Proposed reduction mechanism for the transformation of gold salt (Au³⁺) to gold nanoparticles using *G. biloba* water-soluble extract. The diagram depicts step-by-step reduction processes, where most abundant phytochemicals (ie quercetin) present in the *G. biloba* extract act as reducing agents. The process also highlights the potential role of the extract in capping and stabilizing the newly formed nanoparticles, preventing aggregation and ensuring optimum long-term stability and uniform size distribution.

at pH 4, pH 7, and pH 10, over a month. Remarkably, no significant shifts in the SPR peaks were observed during this time frame. Hydrodynamic size changes in various biological media monitored for a week were negligible, with a variation in size within a 10% (or less) range for various GB-AuNPs (Figure 5).

TEM and Size Distribution

The physicochemical characteristics of GB-AuNPs evaluated by Zetasizer revealed hydrodynamic sizes of 137±6 nm and a low polydispersity index (PDI) of 0.3. The zeta potential of GB-AuNPs was −34 mV, as shown in Figure 6. Additionally, the gold concentration in these GB-AuNPs was quantified to be 277 ppm using ICP-MS, which compared well with the initial amount of $NaAuCl_4 \cdot 2H_2O$ utilized in the synthesis of nanoparticles. The TEM images provided insight into the core size of GB-AuNPs, with an average core size of 19±4 nm (Figure 7). The average core size was determined through size distribution analysis using the Image J.JS software. Notably, the TEM images also demonstrated that the GB-AuNPs exhibited a uniform and spherical morphology, indicating a high degree of monodispersity. Furthermore, the stability of GB-AuNPs in various biological (0.5% BSA, HSA, and Cys, 0.2 M His, 1% NaCl, RPMI and DMEM media, PBS at pH 4, pH 7, and pH 10) revealed limited to no changes in the size and morphological differences as elucidated through extensive TEM analysis of images of GB-AuNPs in various biological media as shown in Figure 8.

Fourier-Transform Infrared Spectroscopy (FTIR)

The gold nanoparticles (GB-AuNPs) FTIR absorption data for GB-AuNPs corresponded to both gum arabic and *G. biloba* phytoextracts (Figure 9). Interestingly, the absorption bands from gum arabic and the phytoextract were quite similar and had some overlap. O-H stretching was observed at approximately 3400 cm⁻¹ and C-H stretching was observed at approximately 2900 cm⁻¹. the ~1600 cm⁻¹ peak and ~1400 cm⁻¹ corresponding to COOH stretching
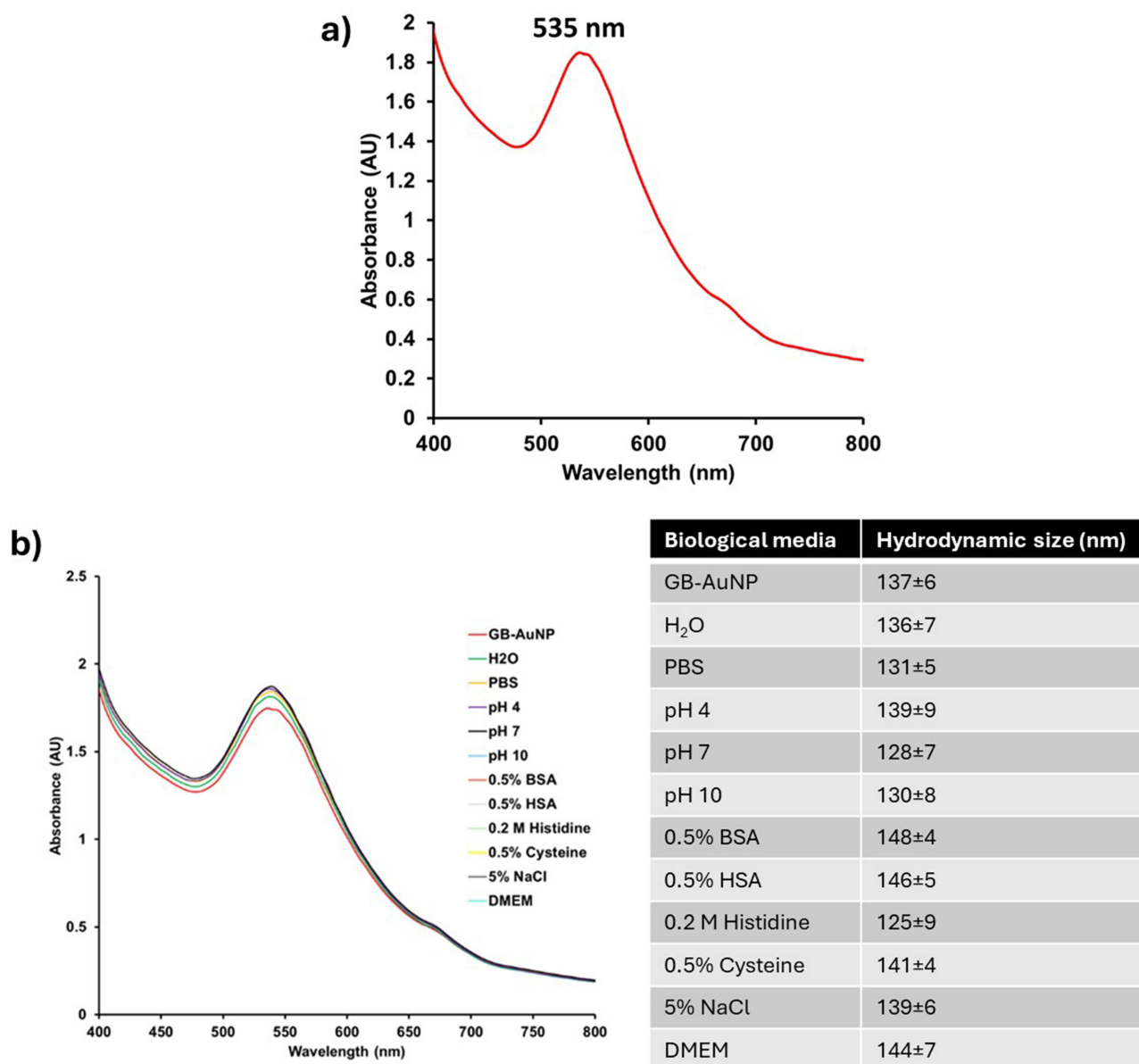
Figure 5 Ultraviolet-visible spectra of (**a**) GB-AuNPs, and (**b**) in vitro stability across various biological media over one month (n=3). Graphics also depict minimal/no variations in size of GB-AuNPs in various biological media a week post-incubation, indicating excellent in vitro stability of GB-AuNPs nanoparticles over time.

and O-H bending, respectively. The peak at ~1100 cm^{-1} peak corresponds to C-O stretching. These results indicate the presence of functional groups in gum arabic and the phytoextract. Minor changes in phytochemical peaks in all the FT-IR spectra of GB-AuNPs confirm oxidation of phytochemicals while they reduced gold in +3 oxidation to corresponding gold nanoparticles.

Powder X-Ray Diffraction (PXRD)

PXRD analysis of the GB-AuNPs revealed four prominent peaks at 2θ values of 38.2°, 44.3°, 64.6°, and 77.5° (Figure 10). These peaks align with the standard Bragg reflections of the (111), (200), (220), and (311) planes of the face-centered cubic (fcc) lattice structure of gold. The alignment of these peaks with the standard fcc gold pattern indicates that the GB-AuNPs have a crystalline gold core with a high degree of structural order. The sharpness and the
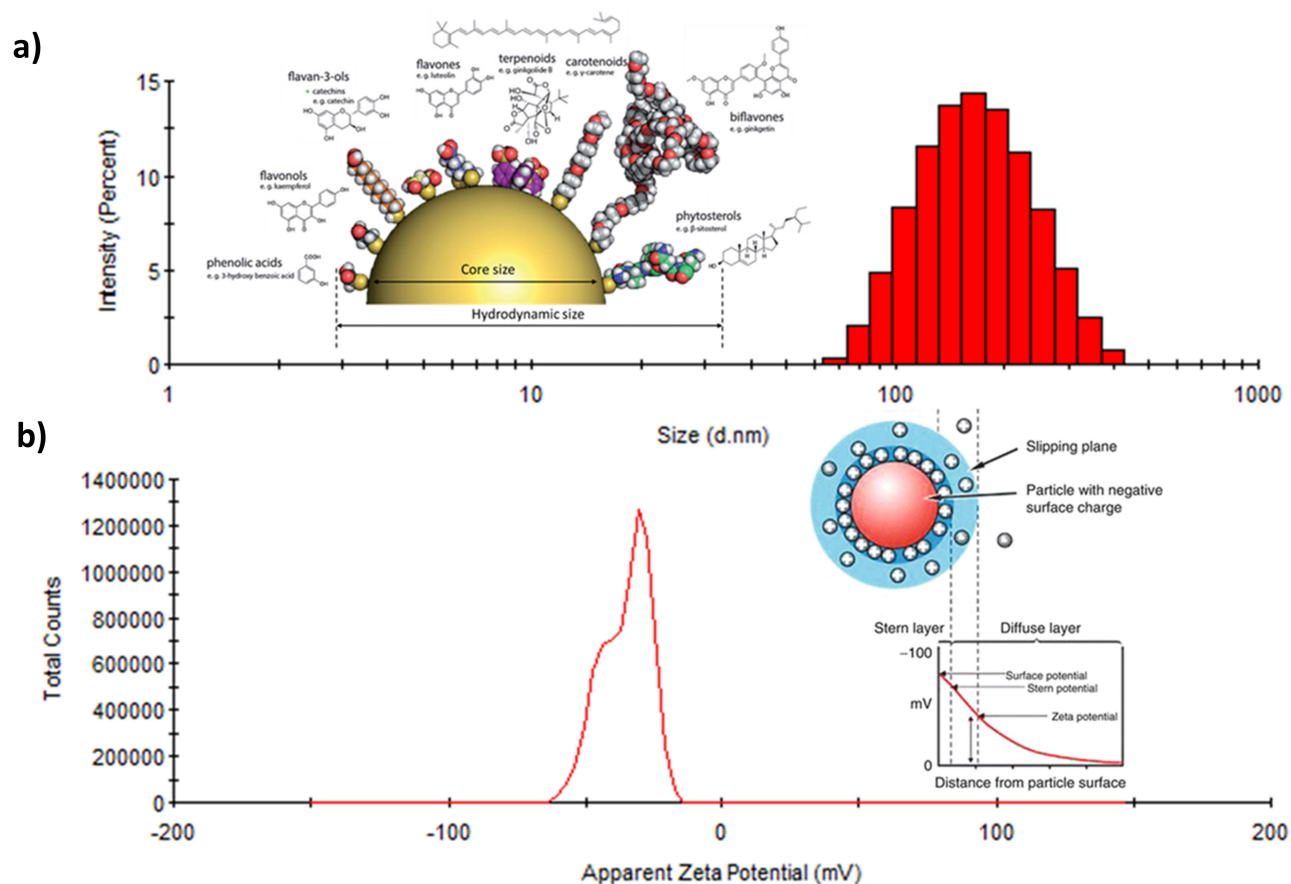
Figure 6 Physicochemical properties of *G. biloba*-synthesized gold nanoparticles (GB-AuNPs): (**a**) hydrodynamic size distribution, and (**b**) zeta potential measurements (n=3). These properties are critical indicators of optimum in vitro stability of GB-AuNPs nanoparticles, their dispersion, and potential interactions in biological environments.

intensity of peaks suggest a high crystallinity and purity of gold nanoparticles, while the absence of additional peaks indicates the absence of significant impurities or secondary phases.

Cellular Internalization of GB-AuNPs

As illustrated in Figures 11a and 12, GB-AuNPs exhibited a remarkable capacity for internalization into breast tumor (MDAMB-231) cells and macrophage (RAW 264.7) cells. This suggests that GB-AuNPs not only possess tumor-specific properties, but also have the ability to target macrophages, which is attributed to increased internalization (Figure 11b). The abundance of *G. biloba* phytoconstituents attached to the expansive surface area of gold facilitates the delivery of a substantial payload of therapeutic phytochemicals, thereby enhancing the uptake of therapeutic nanoparticles by tumor cells.

To underscore the tumor specificity of GB-AuNPs, we have examined their cellular uptake in normal cells (HAEC). The results, as depicted in Figure 11c, indicated that HAEC cells exhibited minimal to no uptake of GB-AuNPs. Additionally, electron microscopy further validated the tumor specificity of the GB-AuNPs, showing a significant propensity for selective internalization into breast tumor (MDAMB-231) cells while sparing normal cells (HAEC cells). This is clear from the presence of vacuoles housing GB-AuNPs through endocytosis, as shown in Figure 12. Furthermore, size distribution analysis of internalized GB-AuNPs revealed an average size of 17±6 nm in MDAMB-231 cell line. This observation unequivocally validates the ability of GB-AuNPs to maintain their structural integrity (size and shape) inside cells, emphasizing their stability. This remarkable stability is evident from the presence of intact nanoparticles with well-defined boundaries, indicating no degradation or aggregation inside
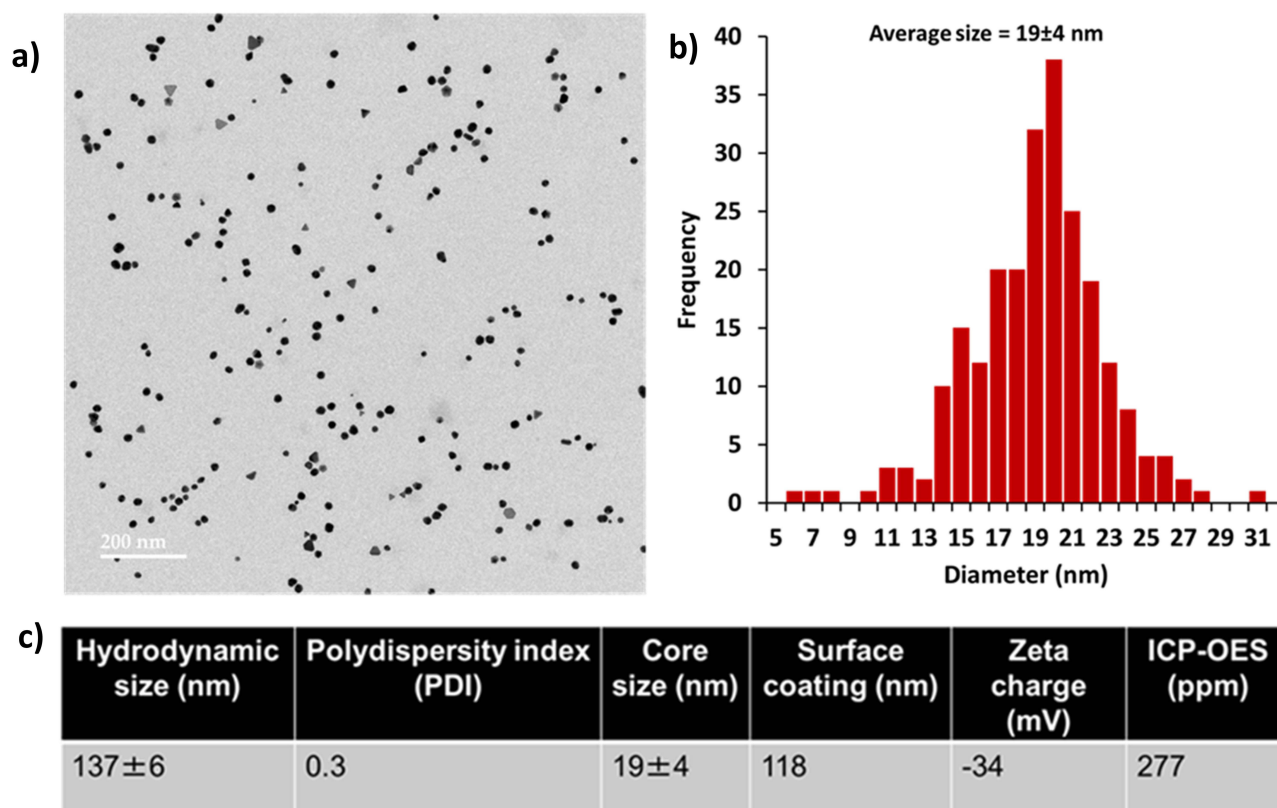
Figure 7 TEM images of (**a**) GB-AuNPs, showcasing well-dispersed spherical nanoparticles, (**b**) size distribution analysis, indicating an average particle size of 19±4 nm, and (**c**) summative data table detailing the gold concentration in nanoparticle solutions.

the complex cellular environment. These findings hold significant promise for the potential use of GB-AuNPs as tumor-cell based and tumor-specific therapeutic agents, with minimal or no toxicity to normal cells.

Antitumor Efficacy of GB-AuNPs

Consistent with our commitment to avoid animal testing, we assessed the in vitro antitumor efficacy of GB-AuNPs using breast (MDAMB-231) cancer cell lines to evaluate their potential for inhibiting tumor cell growth. Cisplatin, an FDA-approved metal-based chemotherapeutic agent, was used as a positive control. Detailed results of antitumor assays presented below unequivocally established that the therapeutic efficacy against tumors was dose dependent. GB-AuNPs exhibited robust antitumor activity, demonstrating potency similar to that of cisplatin at 48 hr post-incubation against MDAMB-321 at half-maximal inhibitory concentration (IC_{50}) values of 37.5 and 42.5 µg/mL, respectively. At 72 hr post-incubation, the IC_{50} of GB-AuNPs was 100 µg/mL whereas for cisplatin it was 25.3 µg/mL. Remarkably, GB-AuNPs exhibited a superior safety profile against normal cells (HAEC) as compared to cisplatin which exhibited an IC_{50} value of 70 and 45 µg/mL at 48 hr and 72 hr post incubation, respectively (Figure 13).

Macrophage Targeting and Immunomodulatory Characteristics of GB-AuNPs

Macrophage infiltration into tumors is a well-known factor associated with poor prognosis and is considered a primary contributor to resistance to chemotherapy and related cancer treatments. Within the tumor microenvironment, tumor-associated macrophages (TAMs) play a pivotal role in initiating rapid angiogenesis and promoting tumor cell migration, leading to invasion and intravasation. TAMs exhibit diminished antigen presentation capabilities and tend to produce increased levels of immunosuppressive cytokines, such as IL-10, and elevated levels of antiangiogenic cytokines, such as IL-6, which is characterized by an immunosuppressive M2 pro-tumor phenotype in most cancers.
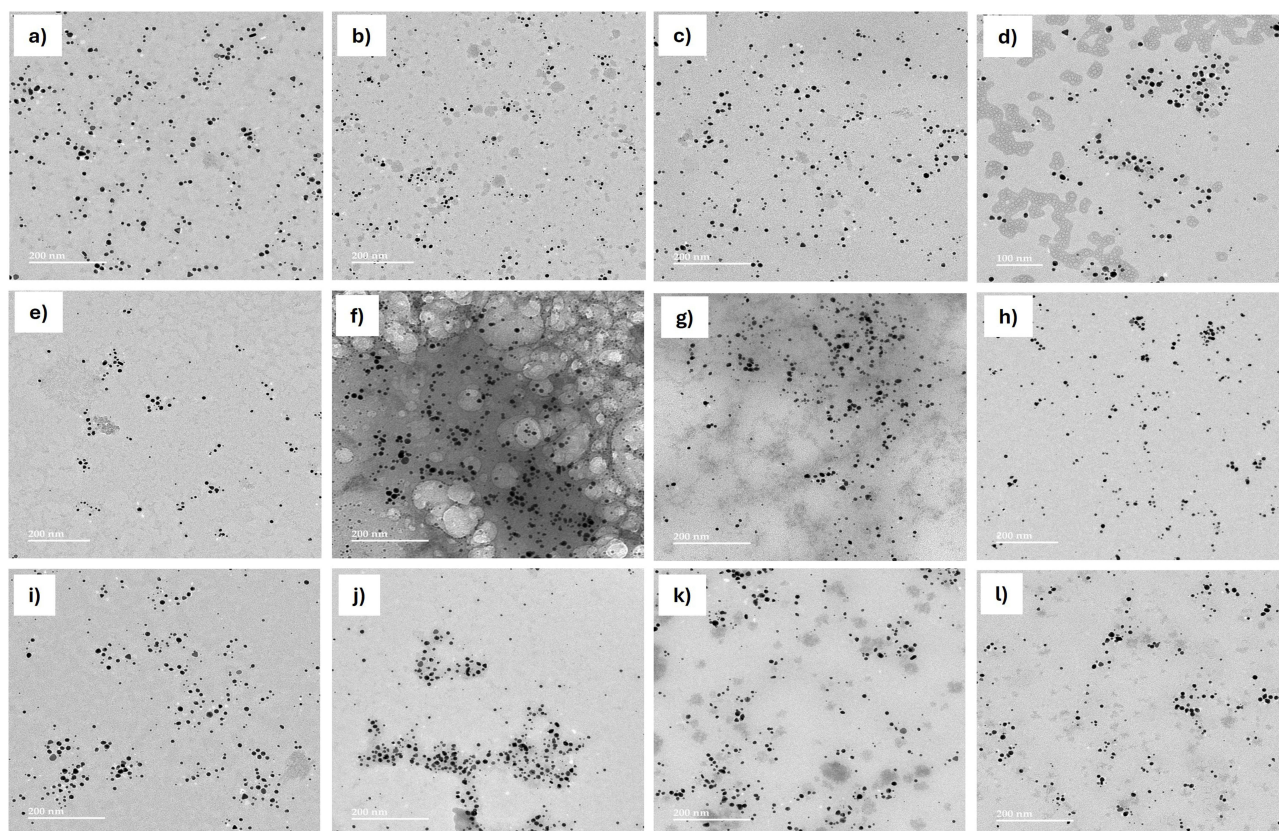
200

Nanotechnology, Science and Applications 2024:17

Figure 8 TEM images of GB-AuNPs in various biological media, including: (**a**) water (H$_2$O), (**b**) phosphate-buffered saline (PBS), (**c**) acidic (pH 4), (**d**) neutral (pH 7), (**e**) basic (pH 10), (**f**) bovine serum albumin (0.5% BSA), (**g**) human serum albumin (0.5% HSA), (**h**) histidine (0.2 M His), (**i**) cysteine (0.5% Cys), (**j**) high-salt (5% NaCl), (**k**) Roswell Park Memorial Institute medium (RPMI), and (**l**) Dulbecco's Modified Eagle's Medium (DMEM).

These processes collectively contribute to immunosuppression at all stages of tumor development, underscoring the importance of targeting pro-tumor macrophages as a crucial therapeutic strategy in cancer treatment. Various types of cancer cells, including breast cancer cells, induce pro-tumor M2 polarization in RAW 264.7 macrophages. Therefore, RAW 264.7 macrophages serve as a reliable model for investigating the targeting abilities of GB-AuNPs, offering valuable insights into the characteristics of cancer macrophage plasticity.

To gain insights into the impact of GB-AuNPs on macrophages, we have investigated the expression of macrophage-polarizing cytokines, including IL-12, IL-10, IL-6, TNF-α, and IFN-γ, when RAW 264.7 macrophages were exposed to GB-AuNPs. Our experimental findings with GB-AuNPs unequivocally demonstrated an increase in the levels of antitumor cytokines, such as IL-12, TNF-α, and IFN-γ, while concurrently decreasing the levels of pro-tumor cytokines, such as IL-10 and IL-6 (Figure 14). The results, as depicted in Figures 11c and 14, unquestionably validated the effective targeting of pro-tumor macrophages by GB-AuNPs. These results strongly suggest the potential immunotherapeutic role of GB-AuNPs prompting further exploration of their capabilities as a new class of nano-ayurvedic medicine agents for modulating macrophage behavior.

Discussion

Our overarching objective of this investigation was to validate the hypothesis that phytochemicals found in the ayurvedic plant *G. biloba* can be used in the form of encapsulated gold nanoparticles towards the development of a new class of nano-ayurvedic medicine products. The highly electron-rich bioactive phytochemicals in *G. biloba* reduced gold in the +3-oxidation state to the corresponding AuNPs in near quantitative yields (Scheme 1 and Figure 1). This green nanotechnology process, pioneered by Katti et al, is unique because the production of AuNPs
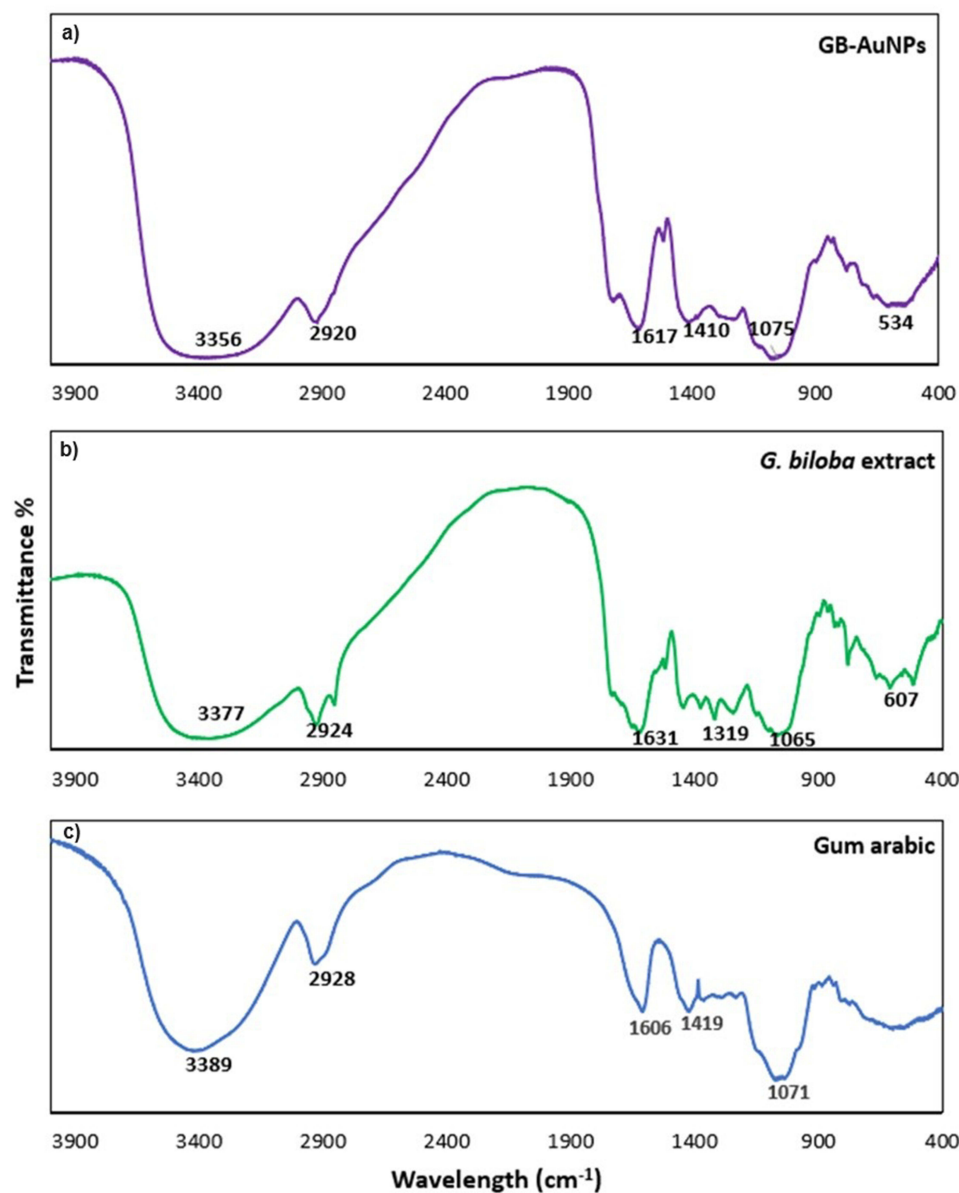
Figure 9 FTIR spectra of (**a**) GB-AuNPs, (**b**) *G. biloba* extract, and (**c**) gum Arabic—reveal characteristic vibrational modes, indicating the presence of specific functional groups capping gold nanoparticle surface. Notably, O-H, COOH stretching, O-H bending, and C-O stretching. These results signify the successful incorporation of hydroxyl, carboxyl, and alkyl groups from the *G. biloba* extract and gum arabic stabilizing and capping GB-AuNPs surface.

occurs without the use of external toxic chemical-based reducing agents. Various phytochemicals, as depicted in Figure 1 and Scheme 1, serve innovative dual roles as reducing and stabilization agents. The UV-Vis spectral data, as shown in Figure 4, confirmed a surface plasmon resonance (SPR) peak at between 535–550 nm, which is a characteristic of AuNPs.[47,49,56,63] The successful production of *G. biloba* gold nanoparticles (GB-AuNPs) using different concentrations *G. biloba* water-soluble extract, illustrated using spectrophotometric and electron micro-scopic techniques, exhibited characteristic SPR absorptions at 535–550 nm for GB-AuNPs (Figure 4a). The physiochemical properties revealed that the 6.25 mg/mL concentration Ginkgo biloba was optimal for the production of well-defined gold nanoparticles exhibiting a zeta potential of −34 mV and a PDI of 0.3—all signifying superior stability and monodispersed morphology as compared to various other concentrations tested. It may be noted that the various other concentrations (as described in the experimental section) produced sub-optimal gold nanoparticles with higher PDI and zeta potentials greater than −30 mV.[64,65]
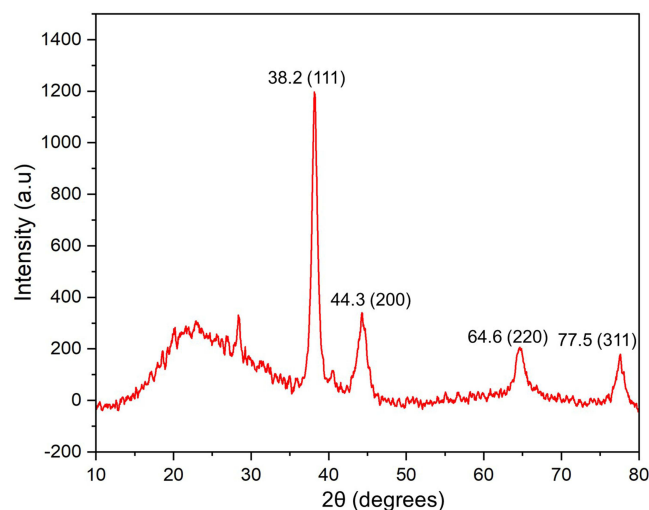
Figure 10 The PXRD spectrum of GB-AuNPs exhibits characteristic Bragg reflections, confirming the crystalline structure of nanoparticles. The diffraction peaks at 2θ values of approximately 38.2°, 44.4°, 64.6°, and 77.5° correspond to the (111), (200), (220), and (311) planes, respectively, of face-centered cubic (fcc) lattice structure of gold.

In order to assess the in vitro stability of GB-AuNPs, we have further challenged these nanoparticles by incubating them in various biological media, including 0.5% BSA, HSA, and Cys, 0.2 M His, 1% NaCl, RPMI and DMEM media, PBS at pH 5, pH 7, and pH 9—over a month. Detailed UV spectral analysis from each of these experiments indicated no significant shifts in the SPR peaks. These results unequivocally suggest robustness of GB-AuNPs in all the above media and highly reliable in vitro stability of these nanoparticles for use in various biomedical applications (Figure 5b). Additionally, the hydrodynamic size changes in various biological media monitored for a week were negligible, with a variation in size within 10% or less for all the GB-AuNPs. These observations corroborate the optimum −34 mV zeta potential, indicative of strong intra and inter particles repulsive forces, for these gold nanoparticles. It is important to recognize that the Derjaguin–Landau–Verwey–Overbeek (DLVO) theory suggests high negative zeta potentials facilitate electrostatic repulsion and steric stabilization and overall significant stability against agglomeration (Figure 6).[66] Our investigations, therefore, provide unequivocal experimental evidence that green nanotechnology routes produce nanomedicinal agents with optimum stability—as shown through extensive TEM images of GB-AuNPs incubated in different biological media (Figure 8). The TEM data, as shown in Figures 7 and 8, demonstrate uniform and spherical morphologies without any agglomeration, confirming monodispersity and optimal GB-AuNPs stability. Hydrodynamic size measurements using dynamic light scattering (DLS) displayed a hydrodynamic size of 137 nm. FTIR analysis revealed the encapsulation of *G. biloba* phytochemicals on gold nanoparticulate surface. It is important to note that *G. biloba* phytochemicals act as both reducing agents as well as capping agents to afford optimal stability to GB-AuNP nanoparticles (Figure 9). The PXRD analysis of AuNPs showed four peaks corresponding to the standard Bragg reflections (111), (200), (220), and (311) planes of the face-centered cubic lattice of crystalline AuNPs (Figure 10).

In order to investigate the tumor cell-targeting capabilities of GB-AuNPs, we have performed incubation of nanoparticles with breast cancer cells (MDAMB-231) and macrophages (RAW 264.7). Confocal microscopy analysis was performed to assess whether AuNPs functionalized with *Ginkgo biloba* phytochemicals (GB-AuNPs) could effectively target both tumor cells and macrophages. The imaging data presented in Figure 11 demonstrate that the GB-AuNPs nano-ayurvedic medicine agent can effectively target both breast tumor cells and macrophages. Furthermore, GB-AuNPs were internalized within these cells, possibly through endocytosis, residing within vacuoles, while preserving their structural integrity in terms of size and shape (Figure 12).

MTT cell proliferation assays were conducted using GB-AuNPs, breast cancer cells (MDAMB-231) and macrophages (RAW 264.7). The results, illustrated in Figure 13, highlight the impressive antitumor efficacy of GB-AuNPs
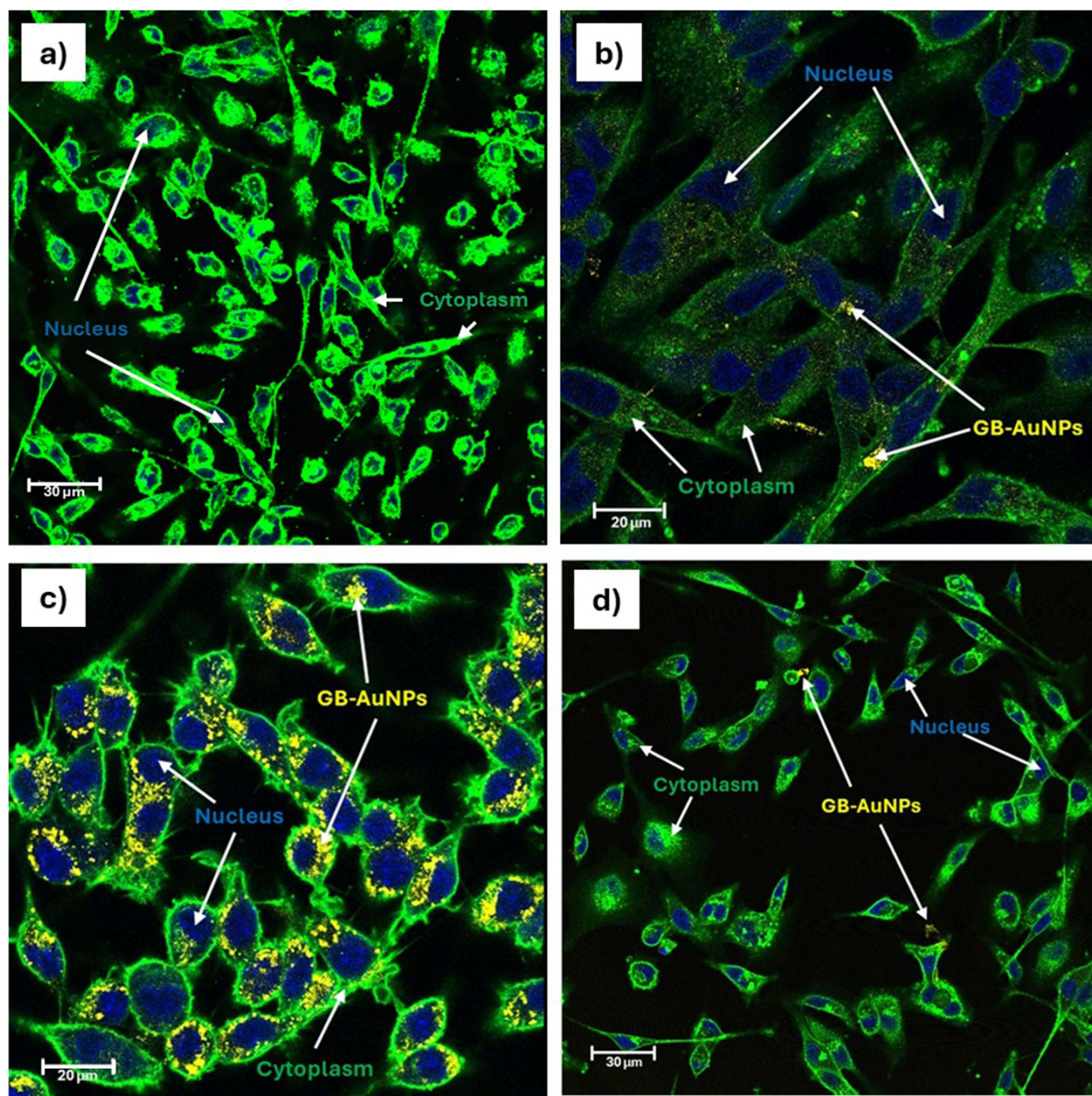
Figure 11 Fluorescence microscopy images showing cellular internalization of GB-AuNPs in different cell types after 24 hr post-incubation. The images display: (**a**) untreated control cells, (**b**) GB-AuNPs-treated breast cancer cells (MDA-MB-231), (**c**) GB-AuNPs-treated murine macrophage cells (RAW 264.7), and (**d**) GB-AuNPs-treated human aortic endothelial cells (HAEC). Cell nuclei are stained with DAPI (blue), while the cytoplasm is stained with wheat germ agglutinin (WGA, green). The presence of GB-AuNPs within the cells indicates successful internalization and endocytosis, which is a crucial step for their potential applications in cancer therapy, imaging, and allied biomedical applications.

against both human aortic endothelial cells and breast tumors. It is worth emphasizing that GB-AuNPs demonstrated a comparable level of antitumor effectiveness when compared to the FDA-approved cisplatin cancer therapeutic agent at 48 hr post-incubation against MDAMB-321 at half-maximal inhibitory concentration (IC_{50}) values of 37.5 and 42.5 µg/mL, respectively (Figure 13). At 72 hr post-incubation, the IC_{50} of GB-AuNPs was 100 µg/mL whereas for cisplatin, it was 25.3 µg/mL. It is well known that cisplatin destroys normal cells and cancer cells indiscriminately. Therefore, the discovery of cancer therapy agents that are selective to tumor cells with minimal toxicity to
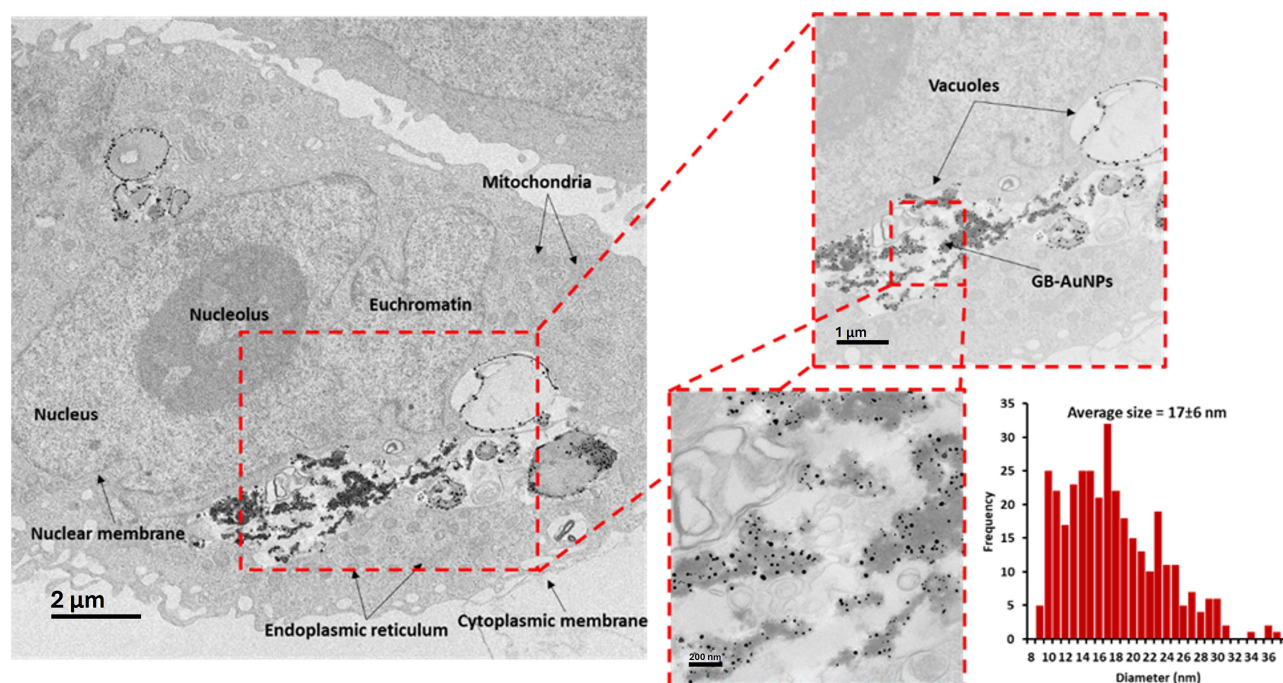
Figure 12 TEM image showing cellular internalization of GB-AuNPs in MDA-MB-231 breast cancer cells after 24 hr post-incubation. Notably, the GB-AuNPs maintain their structural integrity, preserving their original size, morphology and shape within the complex cellular environment.

normal cells is vitally important. Breast Cancer inherits a heterogeneous group of malignancies, each characterized by distinct molecular profiles and responses to treatment.[67] The two cell lines commonly used in breast cancer research are MDAMB-231 and MCF-7, each expressing vastly different subtypes of breast cancers. MDAMB-231 cells arise from triple-negative breast cancer (TNBC), a subtype characterized by the absence of the estrogen receptor (ER), progesterone receptor (PR), and human epidermal growth factor receptor 2 (HER2). In contrast, MDAMB-231 cells, typically exhibit aggressive behavior and tend to show resistance to conventional therapies.[67–70] MCF-7 represents positive (ER+) breast cancer and tends to exhibit a less aggressive behavior. Understanding the differences between the two cell lines is essential for understanding the mechanisms of breast cancer progression and optimizing therapeutic efficiency.[68,70]

A significant finding from the aforementioned investigations is that GB-AuNPs nano-ayurvedic medicine agent exhibited a distinctive ability to selectively target tumor cells while sparing normal cells, suggesting its potential to reduce the systemic toxicity associated with conventional cancer therapeutic agents, such as cisplatin. The FDA-approved cisplatin cancer therapy agent displayed non-selective toxicity to normal cells, affecting both tumor and normal cells (Figure 13). The antitumor efficacy of this nanomedicine agent has revealed strong antitumor effects of GB-AuNPs towards MDAMB-231 cells, which are comparable to those of the FDA-approved cancer therapy agent cisplatin. However, GB-AuNPs exhibited no significant toxic effects on noncancerous, aortic endothelial cells (HAEC). Cytokine measurement studies performed using RAW 264.7 cells, treated with GB-AuNPs, exhibited downregulation in the expression of pro-tumor cytokines (IL-6 and IL-10) with concomitant upregulation of antitumor cytokines (TNF-α, IFN-γ and IL-12) in LPS-induced inflammation as shown in Figure 14.

Our investigations provide unequivocal evidence that green nanotechnology approaches, as described in this study, have resulted in the development of a new nano-ayurvedic medicine agent capable of treating tumors through an immunomodulatory mechanism. Tumor-associated macrophages (TAMs) prominently overexpress immune cell components including CD206, CD163, and CD204. These cellular domains orchestrate multitude of stromal responses within the tumor microenvironment (TME). In some acute cases, TAMs account for > 50% of the
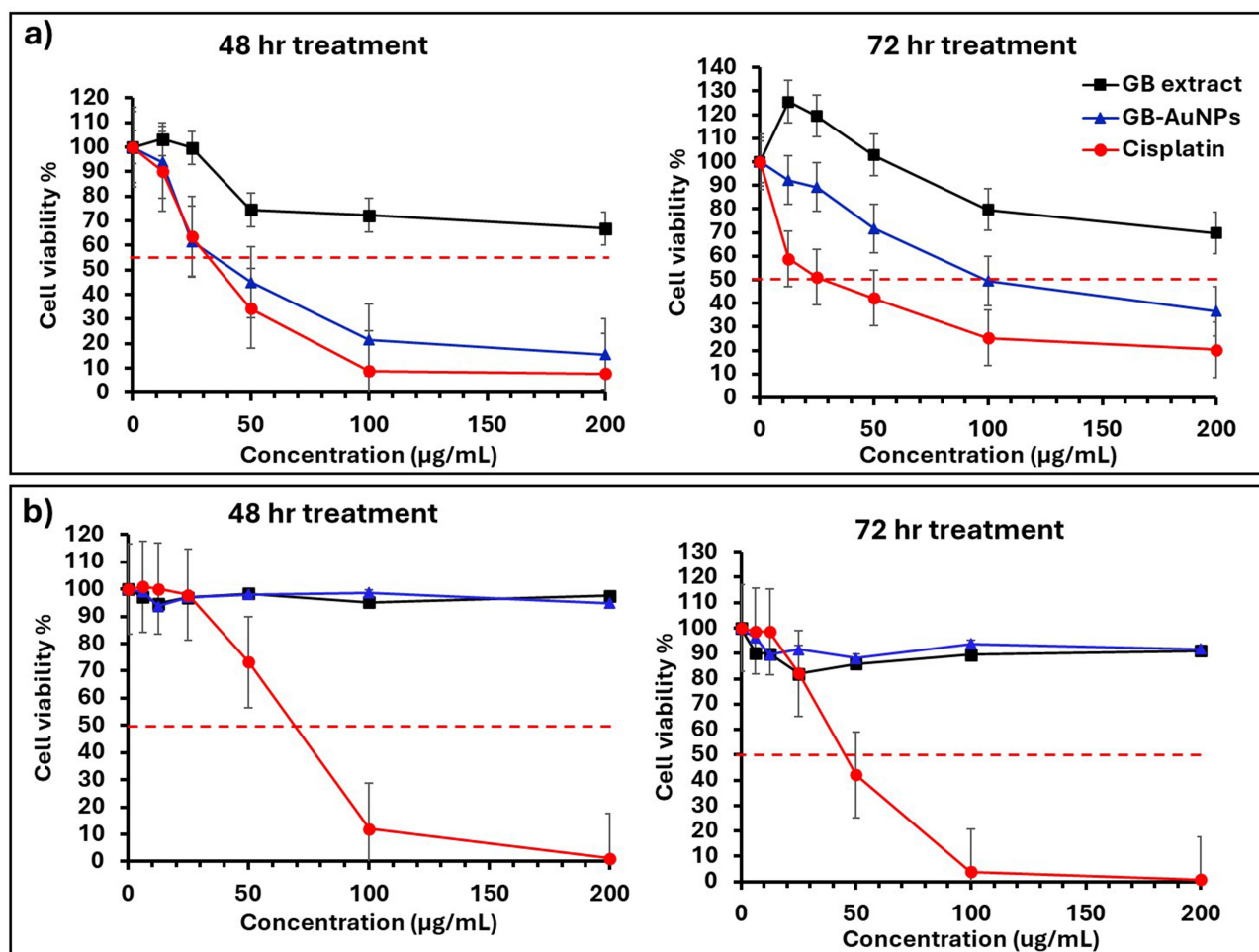
Figure 13 Anticancer efficacy of GB-AuNPs against (**a**) breast cancer cells (MDA-MB-231) and (**b**) human aortic endothelial cells (HAEC) at 48 and 72 hr post-treatment. GB-AuNPs exhibited potent anticancer activity against MDA-MB-231 cells (IC$_{50}$: 37.5–100 µg/mL) and a superior safety profile against HAEC cells, outperforming cisplatin (IC$_{50}$: 25.3–70 µg/mL). Data are expressed as mean optical density ± SEM (n = 3).

tumor mass. TAMs are the main sources of pro-tumor cytokines, such as IL-10, and pro-tumor mitogens that trigger the initiation and progression of cancers. Therefore, TAMs populations are directly related to worse clinical outcomes and, ultimately, to the transformation of disease drug resistance. Tumor microenvironments predispose the recruitment and polarization of macrophages to the tumor site, thus promoting tumor growth, accelerating tumor angiogenesis, expediting and facilitating tumor cell migration, and ultimately creating a favorable environment for extensive colonization and evasion of tumor cells. Therefore, cancer therapy drugs should target pro-tumor (M2 phenotype) macrophages. Macrophage cells RAW 264.7, by default, are considered M2-like macrophages, which are mainly responsible for the promotion, progression, angiogenesis, and metastasis of most tumors. In our study, we used RAW 264.7 macrophages to test whether GB-AuNPs could effectively target these pro-tumor macrophages. As shown in Figures 11c and 14, the new nanomedicine agent, GB-AuNPs, effectively targeted macrophages with an excellent propensity for internalization within macrophage cells. The macrophage-targeting ability of GB-AuNPs nanomedicine agent translates into an excellent therapeutic efficacy of this agent in suppressing the growth of breast tumor cells, as shown above. Therefore, this new nano-ayurvedic agent is an effective immunomodulatory agent for the treatment of breast and various human tumors.
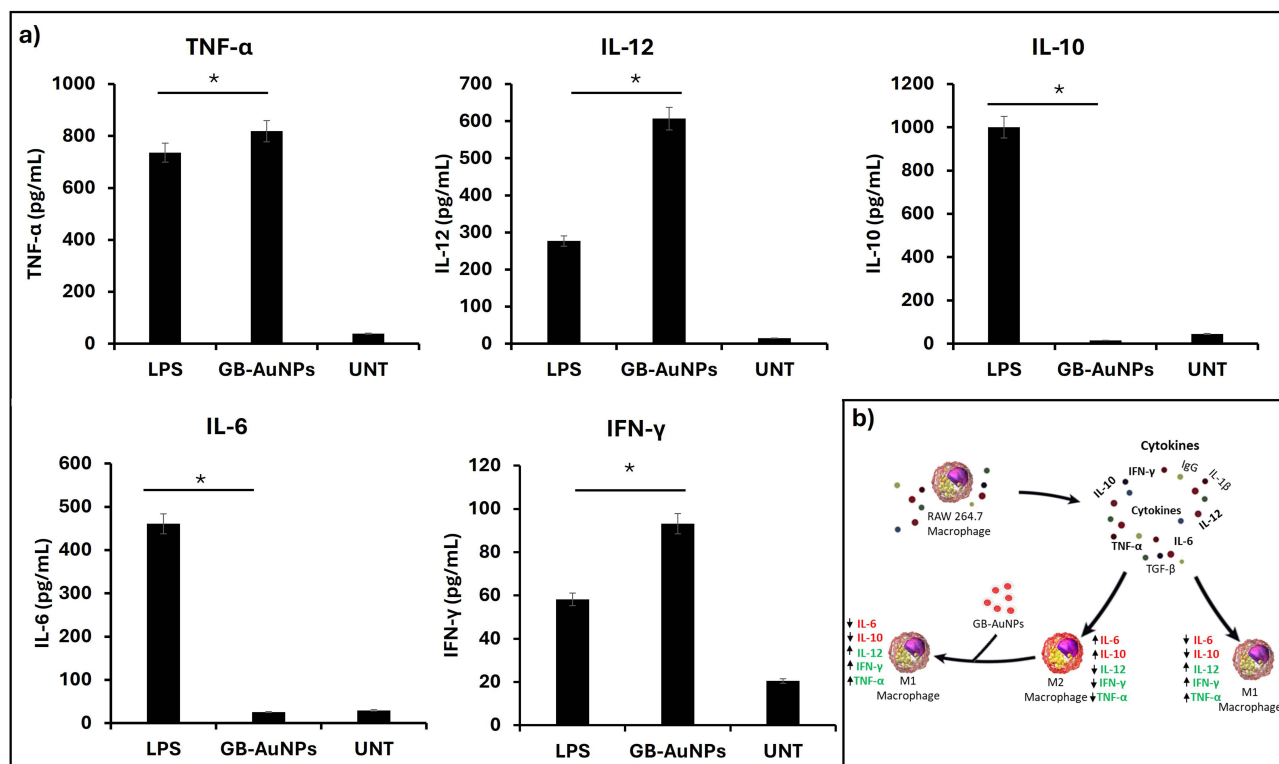
Figure 14 Modulation of cytokine expression by GB-AuNPs in LPS-induced RAW 264.7 macrophages. (**a**) GB-AuNPs suppressed pro-tumor cytokines (IL-6 and IL-10) while enhancing anti-tumor cytokines (TNF-α, IFN-γ, and IL-12), indicating a shift towards an anti-tumor immune response. (**b**) GB-AuNPs promoted M1-like macrophage polarization, characterized by increased expression of pro-inflammatory cytokines. Untreated (UNT) cells served as control. Data represent mean ± SEM from three independent experiments. *P < 0.05 vs the LPS group, indicating statistically significant differences.

Conclusion

Our extensive aforementioned investigations have revealed that the overall phytochemical content, as shown in Figures 1–3 remain almost similar in both fresh and dry leaves of the *Ginkgo biloba* tree. Fallen leaves from the *G. biloba* tree are considered as environmentally friendly by-product of this natural habitat. Therefore, our green nanotechnology approach to produce gold nanoparticles, as described in this investigation, is a net carbon zero or net carbon negative process to develop a new generation of Nano-Ayurvedic medicine products. The aforementioned results and discussions provide compelling evidence supporting the potential use of phytochemicals derived from *Ginkgo biloba* in the synthesis of gold nanoparticles (GB-AuNPs) with immunomodulatory properties. Cis platin is FDA approved—considered as a "work horse" in treating most human cancers. As this drug destroys cancerous and normal cells indiscriminately, most patients post treatment suffer from severely compromised immune system. In this context, our discovery of immunomodulatory capabilities of GB-AuNPs which boost the immune system, while treating tumors, is a significant finding in pursuit of immunotherapy of cancers. Therapeutic efficacy in tumor cells was achieved without any adverse effects observed in normal human aortic endothelial cells (HAEC), thus highlighting the selective cytotoxicity and immunomodulatory features of GB-AuNPs towards cancerous cells.

Acknowledgments

the training program NANOMED EMJMD. We also acknowledge the Botanical Garden of the Department of Pharmacy, Faculty of Health, University of Angers for providing samples of *G. biloba* for this investigation.

Disclosure

The authors (s) report no conflicts of interest.

References

1. Boateng ID. Ginkgols and bilobols in ginkgo biloba L. A review of their extraction and bioactivities. *Phytother Res*. 2023;37(8):3211–3223. doi:10.1002/ptr.7877
2. Šamec D, Karalija E, Dahija S, Hassan STS. Biflavonoids: important contributions to the health benefits of ginkgo (Ginkgo biloba L.). *Plants*. 2022;11(10). doi:10.3390/plants11101381
3. Liu Q, Chen L, Yin W, Nie Y, Zeng P, Yang X. Anti-tumor effect of ginkgetin on human hepatocellular carcinoma cell lines by inducing cell cycle arrest and promoting cell apoptosis. *Cell Cycle*. 2022;21(1):74–85. doi:10.1080/15384101.2021.1995684
4. Yuan Z, Tian Y, He F, Zhou H. Endophytes from Ginkgo biloba and their secondary metabolites. *ChinMed*. 2019;14(1). doi:10.1186/s13020-019-0271-8
5. Shanmugam MK, Garg M, Makhija P, et al. Ginkgolic acids confer potential anticancer effects by targeting pro- inflammatory and oncogenic signaling molecules. *Curr Mol Pharmacol*. 2021;14(5):806–822. doi:10.2174/1874467214666210126112413
6. Cao C, Su Y, Gao Y, et al. Ginkgo biloba exocarp extract inhibits the metastasis of B16-F10 melanoma involving PI3K/Akt/NF- B/MMP-9 signaling pathway. *Evid Based Complement Alternat Med*. 2018;2018. doi:10.1155/2018/4969028
7. Feodorova Y, Tomova T, Minchev D, Turiyski V, Draganov M, Argirova M. Cytotoxic effect of Ginkgo biloba kernel extract on HCT116 and A2058 cancer cell lines. *Heliyon*. 2020;6(9):e04941. doi:10.1016/j.heliyon.2020.e04941
8. Chen P, Wang T, Chen Q. Ginkgo biloba golden leaf extract (GGLE) inhibits melanoma cell invasion and angiogenesis through inhibition of angiogenin. *Integr Cancer Ther*. 2023;22. doi:10.1177/15347354221134513
9. Barbalho SM, Direito R, Laurindo LF, et al. Ginkgo biloba in the aging process: a narrative review. *Antioxidants*. 2022;11(3). doi:10.3390/antiox11030525
10. Ahmed HH, Shousha WG, El-Mezayen HA, El-Toumy SA, Sayed AH, Ramadan AR. Biochemical and molecular evidences for the antitumor potential of Ginkgo biloba leaves extract in rodents. *Acta Biochim Pol*. 2017;64(1):25–33. doi:10.18388/abp.2015_1200
11. Demoret RM, Baker MA, Ohtawa M, et al. Synthetic, mechanistic, and biological interrogation of Ginkgo biloba chemical space en route to (-)-bilobalide. *J Am Chem Soc*. 2020;142(43):18599–18618. doi:10.1021/jacs.0c08231
12. Wang M, Li R, Bai M, Zhou X. Exploration of Ginkgo biloba leaves on non-small cell lung cancer based on network pharmacology and molecular docking. *Medicine*. 2024;103(9):E37218. doi:10.1097/MD.0000000000037218
13. Zhang Z, Chen S, Mei H, et al. Ginkgo biloba leaf extract induces DNA damage by inhibiting topoisomerase II activity in human hepatic cells. *Sci Rep*. 2015;5:1–13. doi:10.1038/srep14633
14. Singh SK, Srivastav S, Castellani RJ, Plascencia-Villa G, Perry G. Neuroprotective and antioxidant effect of ginkgo biloba extract against ad and other neurological disorders. *Neurotherapeutics*. 2019;16(3):666–674. doi:10.1007/s13311-019-00767-8
15. Nowak A, Kojder K, Zielonka-Brzezicka J, et al. The use of ginkgo biloba l. as a neuroprotective agent in the alzheimer's disease. *Front Pharmacol*. 2021;12:1–18. doi:10.3389/fphar.2021.775034
16. Choi YJ, Alishir A, Jang T, Kang KS, Lee S, Kim KH. Antiskin aging effects of indole alkaloid n-glycoside from ginkgo fruit (Ginkgo biloba fruit) on TNF-α-exposed human dermal fibroblasts. *J Agric Food Chem*. 2022;70(42):13651–13660. doi:10.1021/acs.jafc.2c05769
17. Li M, Li B, Xia ZM. Anticancer effects of five biflavonoids from ginkgo biloba l. male flowers in vitro. *Molecules*. 2019;1–13 doi:10.3390/molecules24081496.
18. Wang R, Shao X, Yang J, Liu Z, Chew L, Shao Y. Ginkgo biloba extract mechanism inhibits hepatocellular carcinoma through the nuclear factor-κB/P53 signaling pathway. *J Environ Pathol Toxicol Oncol*. 2020;39(2):179–189. doi:10.1615/JEnvironPatholToxicolOncol.2020034510
19. Zuo W, Yan F, Zhang B, Li J, Mei D. Advances in the studies of Ginkgo biloba leaves extract on aging-related diseases. *Aging Dis*. 2017;8(6):812–826. doi:10.14336/AD.2017.0615
20. Das R, Lami MS, Chakraborty AJ, et al. Ginkgo biloba: a treasure of functional phytochemicals with multimedicinal applications. *Evid Based Complement Alternat Med*. 2022;2022. doi:10.1155/2022/8288818
21. Moriwaki M, Tominaga E, Kito K, et al. Bioavailability of flavonoids in ginkgo biloba extract-γ-cyclodextrin complex. *Nat Prod Commun*. 2023;18(5):1–3. doi:10.1177/1934578X231170221
22. Tsai JR, Liu PL, Chen YH, et al. Ginkgo biloba extract decreases non-small cell lung cancer cell migration by downregulating metastasis-associated factor heat-shock protein 27. *PLoS One*. 2014;9(3). doi:10.1371/journal.pone.0091331
23. Yu J, Wang J, Yang J, et al. New insight into the mechanisms of Ginkgo biloba leaves in the treatment of cancer. *Phytomedicine*. 2024:122. doi:10.1016/j.phymed.2023.155088
24. Chen X, Zeng L. Ginkgo biloba extract 761 enhances 5-fluorouracil chemosensitivity in colorectal cancer cells through regulation of high mobility group-box 3 expression. *Am J Transl Res*. 2018;10(6):1773–1783.
25. Bhosale PB, Ha SE, Vetrivel P, Kim HH, Kim SM, Kim GS. Functions of polyphenols and its anticancer properties in biomedical research: a narrative review. *Transl Cancer Res*. 2020;9(12):7619–7631. doi:10.21037/tcr-20-2359
26. Osman AS, Abu-Risha SE, Bakr SM, et al. Comparative study between effects of ginkgo biloba extract and extract loaded on gold nanoparticles on hepatotoxicity induced by potassium bromate. *Environ Sci Pollut Res*. 2023;30(2):5027–5036. doi:10.1007/s11356-022-22324-1

27. Li Y, Zhu X, Wang K, Zhu L, Murray M, Zhou F. The potential of Ginkgo biloba in the treatment of human diseases and the relationship to Nrf2-mediated antioxidant protection. *J Pharm Pharmacol*. 2022;74(12):1689–1699. doi:10.1093/jpp/rgac036

28. Barani M, Sangiovanni E, Angarano M, et al. Phytosomes as innovative delivery systems for phytochemicals: a comprehensive review of literature. *International Journal of Nanomedicine*. 2021;16:6983–7022. doi:10.2147/IJN.S318416

29. Kaplan A. The nanocomposites designs of phytomolecules from medicinal and aromatic plants: promising anticancer-antiviral applications. *Beni Suef Univ J Basic Appl Sci*. 2022;11(1). doi:10.1186/s43088-022-00198-z

30. Akanchise T, Angelova A. Ginkgo biloba and long covid: in vivo and in vitro models for the evaluation of nanotherapeutic efficacy. *Pharmaceutics*. 2023;15(5). doi:10.3390/pharmaceutics15051562

31. El-Deeb NM, Khattab SM, Abu-Youssef MA, Badr AMA. Green synthesis of novel stable biogenic gold nanoparticles for breast cancer therapeutics via the induction of extrinsic and intrinsic pathways. *Sci Rep*. 2022;12(1). doi:10.1038/s41598-022-15648-y

32. Malik MA, Hashmi AA, Al-Bogami AS, Wani MY. Harnessing the power of gold: advancements in anticancer gold complexes and their functionalized nanoparticles. *J Mater Chem B*. 2023;12(3):552–576. doi:10.1039/d3tb01976d

33. Yusufbeyoğlu S, Cinar V, Ildiz N, Hamurcu Z, Ocsoy İ, Kilic AB. The use of conjugated gold nanorods with reduced toxicity in photothermal therapy for MRSA. *ChemistrySelect*. 2024;9(11). doi:10.1002/slct.202304893

34. Mal S, Chakraborty S, Mahapatra M, et al. Tackling breast cancer with gold nanoparticles: twinning synthesis and particle engineering with efficacy. *Nanoscale Adv*. 2024;6(11):2766–2812. doi:10.1039/d3na00988b

35. Abed AS, Khalaf YH, Mohammed AM. Green synthesis of gold nanoparticles as an effective opportunity for cancer treatment. *Results Chem*. 2023;5. doi:10.1016/j.rechem.2023.100848

36. Katti K, Cutler C, Khoobchandani M, Katti K. Mangiferin encapsulated gold nanoparticles, fabrication methods and cancer therapeutic methods. 2022;2.

37. Katti K, Khoobchandani M, Katti K, Joshi C, Khan A, Mutalik V. Ayurvedic encapsulated gold nanoparticles, fabrication methods and cancer therapeutic methods. 2023;2.

38. Khoobchandani M, Katti KK, Karikachery AR, Thipe VC, Bloebaum PLR, Katti KV. Targeted Phytochemical-Conjugated Gold Nanoparticles in Cancer Treatment BT. In: Khoobchandani M, Saxena A editors. *Biotechnology Products in Everyday Life*. Springer International Publishing; 2019:37–52. doi:10.1007/978-3-319-92399-4_3

39. Canha De MN, Thipe VC, Katti KV, et al. The activity of gold nanoparticles synthesized using helichrysum odoratissimum against cutibacterium acnes biofilms. *Front Cell Dev Biol*. 2021;9(September):1–16. doi:10.3389/fcell.2021.675064

40. Lambrechts IA, Thipe VC, Katti KV, et al. Targeting acne bacteria and wound healing in vitro using Plectranthus aliciae, rosmarinic acid, and tetracycline gold nanoparticles. *Pharmaceuticals*. 2022;15(8). doi:10.3390/ph15080933

41. Sibuyi NRS, Thipe VC, Panjtan-Amiri K, et al. Green synthesis of gold nanoparticles using acai berry and elderberry extracts and investigation of their effect on prostate and pancreatic cancer cells. *BJGP Open*. 2021;8:1–8. doi:10.1177/1849543521995310

42. Khoobchandani M, Khan A, Katti KVKK, et al. Green nanotechnology of MGF-AuNPs for immunomodulatory intervention in prostate cancer therapy. *Sci Rep*. 2021;11(1):16797. doi:10.1038/s41598-021-96224-8

43. Khoobchandani M, Katti KK, Karikachery AR, et al. New approaches in breast cancer therapy through green nanotechnology and nano-ayurvedic medicine - pre-clinical and pilot human clinical investigations. *Int J Nanomed*. 2020;15:181–197. doi:10.2147/IJN.S219042

44. Katti KK, Kattumuri V, Bhaskaran S, Katti KV, Kannan R. Facile and general method for synthesis of sugar-coated gold nanoparticles. *Int J Green Nanotechnol Biomed*. 2009;1(1):B53–B59. doi:10.1080/19430850902983848

45. Shukla R, Nune SK, Chanda N, et al. Soybeans as a phytochemical reservoir for the production and stabilization of biocompatible gold nanoparticles. *Small*. 2008;4(9):1425–1436. doi:10.1002/smll.200800525

46. Katti KK, Chanda N, Shukla R, et al. Green nanotechnology from cumin phytochemicals: generation of biocompatible gold nanoparticles. *Int J Green Nanotechnol Biomed*. 2009;1(1):B39–B52. doi:10.1080/19430850902931599

47. Geraldes AN, Alves A, Leal J, et al. Green nanotechnology from plant extracts: synthesis and characterization of gold nanoparticles. *Adv Nanoparticles*. 2016;176–185.

48. Nune SK, Chanda N, Shukla R, et al. Green nanotechnology from tea: phytochemicals in tea as building blocks for production of biocompatible gold nanoparticles. *J Mater Chem*. 2009;19(19):2912–2920. doi:10.1039/B822015H

49. Gamal-Eldeen AM, Moustafa D, El-Daly SM, et al. Gum Arabic-encapsulated gold nanoparticles for a non-invasive photothermal ablation of lung tumor in mice. *Biomed. Pharmacother*. 2017;89:1045–1054. doi:10.1016/j.biopha.2017.03.006

50. Kattumuri V, Katti KK, Bhaskaran S, et al. Gum arabic as a phytochemical construct for the stabilization of gold nanoparticles: in vivo pharmacokinetics and X-ray-contrast-imaging studies. *Small*. 2007;3(2):333–341. doi:10.1002/smll.200600427

51. Katti KV. Realms of green nanotechnology. *Int J Green Nanotech*. 2013;5(1):1. doi:10.1177/1943089213509648

52. Thipe VC, Karikachery AR, Çakılkaya P, et al. Green nanotechnology—An innovative pathway towards biocompatible and medically relevant gold nanoparticles. *J Drug Deliv Sci Technol*. 2022;70. doi:10.1016/j.jddst.2022.103256

53. De Canha MN, Thipe VC, Katti KV, et al. The activity of gold nanoparticles synthesized using helichrysum odoratissimum against cutibacterium acnes biofilms. *Front Cell Dev Biol*. 2021;9(September):1–16. doi:10.3389/fcell.2021.675064

54. Hans CP, Sharma N, Downey E, Khoobchandani M, Katti K, Katti KV. Mangiferin conjugated gold nanoparticles protect against the development of abdominal aortic aneurysm in an apoe−/− mouse model. *JVS Vasc Sci*. 2022;16–17. doi:10.1016/j.jvssci.2022.05.038

55. Chanda N, Kattumuri V, Shukla R, et al. Bombesin functionalized gold nanoparticles show in vitro and in vivo cancer receptor specificity. *Proc Natl Acad Sci U S A*. 2010;107(19):8760–8765. doi:10.1073/pnas.1002143107

56. Thipe VC, Amiri KP, Bloebaum P, et al. Development of resveratrol-conjugated gold nanoparticles: interrelationship of increased resveratrol Corona on anti-tumor efficacy against breast, pancreatic and prostate cancers. *Int J Nanomed*. 2019;14:4413–4428. doi:10.2147/IJN.S204443

57. Tangthong T, Piroonpan T, Thipe VC, et al. Bombesin peptide conjugated water-soluble chitosan gallate—a new nanopharmaceutical architecture for the rapid one-pot synthesis of prostate tumor targeted gold nanoparticles. *Int J Nanomed*. 2021;16(October):6957–6981. doi:10.2147/IJN.S327045

58. Khoobchandani M, Zambre A, Katti KVK, ho LC, Katti KVK. Green nanotechnology from Brassicaceae: development of broccoli phytochemicals – encapsulated gold nanoparticles and their applications in nanomedicine. *I J Green Nanotech*. 2013. doi:10.1177/1943089213509474

59. Katti K, Khan A, Mutalik V. Ayurvedic encapsulated gold nanoparticles, fabrication methods and cancer therapeutic methods. *US 2021/0008103 A1*. 2021;2021:1–60.

60. Khoobchandani M, Katti K, Maxwell A, Fay WP, Katti KV. Laminin receptor-avid nanotherapeutic EGCg-AuNPs as a potential alternative therapeutic approach to prevent restenosis. *Int J Mol Sci*. 2016;17(3). doi:10.3390/ijms17030316

61. Khoobchandani KVKM, VCTAY A, Katti YKK, et al. Prostate tumor therapy advances in nuclear medicine: green nanotechnology toward the design of tumor specific radioactive gold nanoparticles. *J Radioanal Nucl Chem*. 2018;318(3):1737–1747. doi:10.1007/s10967-018-6320-4

62. Shukla R, Chanda N, Zambre A, et al. Laminin receptor specific therapeutic gold nanoparticles (198AuNP-EGCg) show efficacy in treating prostate cancer. *Proc Natl Acad Sci U S A*. 2012;109(31):12426–12431. doi:10.1073/pnas.1121174109

63. Sibuyi NRS, Thipe VC, Panjtan-Amiri K, Meyer M, Katti KV. Green synthesis of gold nanoparticles using acai berry and elderberry extracts and investigation of their effect on prostate and pancreatic cancer cells. *BJGP Open*. 2021;8:1–8. doi:10.1177/1849543521995310

64. Serrano-Lotina A, Portela R, Baeza P, Alcolea-Rodriguez V, Villarroel M, Ávila P. Zeta potential as a tool for functional materials development. *Catal Today*. 2023;423. doi:10.1016/j.cattod.2022.08.004

65. Németh Z, Csóka I, Semnani Jazani R, et al. Quality by design-driven zeta potential optimisation study of liposomes with charge imparting membrane additives. *Pharmaceutics*. 2022;14(9). doi:10.3390/pharmaceutics14091798

66. Agmo Hernández V. An overview of surface forces and the DLVO theory. *ChemTexts*. 2023;9(4). doi:10.1007/s40828-023-00182-9

67. Dai X, Cheng H, Bai Z, Li J. Breast cancer cell line classification and its relevance with breast tumor subtyping. *J Cancer*. 2017;8(16):3131–3141. doi:10.7150/jca.18457

68. Pommerenke C, Nagel S, Haake J, et al. Molecular characterization and subtyping of breast cancer cell lines provide novel insights into cancer relevant genes. *Cells*. 2024;13(4). doi:10.3390/cells13040301

69. Finlay-Schultz J, Jacobsen BM, Riley D, et al. New generation breast cancer cell lines developed from patient-derived xenografts. *Breast Cancer Res*. 2020;22(1). doi:10.1186/s13058-020-01300-y

70. Farhadi P, Yarani R, Valipour E, Kiani S, Hoseinkhani Z, Mansouri K. Cell line-directed breast cancer research based on glucose metabolism status. *Biomed Pharmacother* 2022;146. doi:10.1016/j.biopha.2021.112526